

RESEARCH ARTICLE

Makorin 1 controls embryonic patterning by alleviating Bruno1-mediated repression of *oskar* translation

Annabelle Dold¹, Hong Han², Niankun Liu², Andrea Hildebrandt^{3,4}, Mirko Brüggemann⁵, Cornelia Rücklé^{4,5}, Heike Hänel⁴, Anke Busch⁶, Petra Beli³, Kathi Zarnack⁵, Julian König⁴, Jean-Yves Roignant^{1,7*}, Paul Lasko^{2,8*}

1 RNA Epigenetics, Institute of Molecular Biology, Mainz, Germany, **2** Department of Biology, McGill University, Montréal, Québec, Canada, **3** Chromatin Biology and Proteomics, Institute of Molecular Biology, Mainz, Germany, **4** Genomic Views of Splicing Regulation, Institute of Molecular Biology, Mainz, Germany, **5** Buchmann Institute for Molecular Life Sciences, Goethe University Frankfurt, Frankfurt, Germany, **6** Bioinformatics Core Facility, Institute of Molecular Biology, Mainz, Germany, **7** Center for Integrative Genomics, Génopode Building, Faculty of Biology and Medicine, University of Lausanne, Lausanne, Switzerland, **8** Department of Human Genetics, Radboud University Medical Center, Nijmegen, Netherlands

☯ These authors contributed equally to this work.

* jean-yves.roignant@unil.ch (JYR); paul.lasko@mcgill.ca (PL)



OPEN ACCESS

Citation: Dold A, Han H, Liu N, Hildebrandt A, Brüggemann M, Rücklé C, et al. (2020) Makorin 1 controls embryonic patterning by alleviating Bruno1-mediated repression of *oskar* translation. PLoS Genet 16(1): e1008581. <https://doi.org/10.1371/journal.pgen.1008581>

Editor: Jean-René Huynh, Collège de France CNRS, FRANCE

Received: April 10, 2019

Accepted: December 20, 2019

Published: January 24, 2020

Copyright: © 2020 Dold et al. This is an open access article distributed under the terms of the [Creative Commons Attribution License](https://creativecommons.org/licenses/by/4.0/), which permits unrestricted use, distribution, and reproduction in any medium, provided the original author and source are credited.

Data Availability Statement: The iCLIP data has been deposited to the NCBI's Gene Expression Omnibus and are accessible through GEO Series accession number GSE123052 (<https://www.ncbi.nlm.nih.gov/geo/query/acc.cgi?acc=GSE123052>).

Funding: The initials of the authors who received the awards were PL, JYR, JK, and KZ. PL received grants MOP-44050 and IOP-107945 from the Canadian Institutes of Health Research (CIHR), JYR received grant RO 4681/4-1 from the Deutsche Forschungsgemeinschaft (DFG), JK

Abstract

Makorins are evolutionary conserved proteins that contain C₃H-type zinc finger modules and a RING E3 ubiquitin ligase domain. In *Drosophila*, maternal Makorin 1 (Mkrn1) has been linked to embryonic patterning but the mechanism remained unsolved. Here, we show that Mkrn1 is essential for axis specification and pole plasm assembly by translational activation of *oskar* (*osk*). We demonstrate that Mkrn1 interacts with poly(A) binding protein (pAbp) and binds specifically to *osk* 3' UTR in a region adjacent to A-rich sequences. Using *Drosophila* S2R+ cultured cells we show that this binding site overlaps with a Bruno1 (Bru1) responsive element (BREs) that regulates *osk* translation. We observe increased association of the translational repressor Bru1 with *osk* mRNA upon depletion of Mkrn1, indicating that both proteins compete for *osk* binding. Consistently, reducing Bru1 dosage partially rescues viability and Osk protein level in ovaries from *Mkrn1* females. We conclude that Mkrn1 controls embryonic patterning and germ cell formation by specifically activating *osk* translation, most likely by competing with Bru1 to bind to *osk* 3' UTR.

Author summary

To ensure accurate development of the *Drosophila* embryo, proteins and mRNAs are positioned at specific sites within the embryo. Many of these factors are produced and localized during the development of the egg in the mother. One protein essential for this process that has been heavily studied is Oskar (Osk), which is positioned at the posterior pole. During the localization of *osk* mRNA, its translation is repressed by the RNA-binding protein Bruno1 (Bru1), ensuring that Osk protein is not present outside of the posterior where it is harmful. At the posterior pole, *osk* mRNA is activated

received grant KO 4566/3-2 from the DFG, KZ received funding from the LOEWE program Ubiquitin Networks (Ub-Net) of the State of Hesse (Germany) and grant ZA 881/5-2 from the DFG. The funders had no role in study design, data collection and analysis, decision to publish, or preparation of the manuscript.

Competing interests: The authors have declared that no competing interests exist.

through mechanisms that are not yet understood. In this work, we show that the conserved protein Makorin 1 (Mkrn1) is a novel factor involved in the translational activation of *osk*. Mkrn1 binds specifically to *osk* mRNA, overlapping with a binding site of Bru1, thus alleviating the association of Bru1 with *osk*. Moreover, Mkrn1 is stabilized by poly(A) binding protein (pAbp), a translational activator that binds *osk* mRNA in close proximity to one Mkrn1 binding site. Our work thus helps to answer a long-standing question in the field, providing insight about the function of Mkrn1 and more generally into embryonic patterning in animals.

Introduction

In the *Drosophila* embryo, the maternally deposited pole plasm is a site of specialized translation of mRNAs required for germ cell specification and posterior patterning [1]. Numerous mRNAs accumulate in the pole plasm during oogenesis and early embryogenesis through several different localization mechanisms [2,3]. Among these mRNAs is *oskar* (*osk*), which localizes during oogenesis to the posterior along a polarized microtubule network [4] and via a trapping mechanism [5]. Several lines of evidence indicate that *osk* is the primary determinant that specifies germ cells and posterior patterning. Ectopic expression of *osk* at the anterior can induce a second set of pole cells and a bicaudal embryonic segmentation pattern with mirror-image posterior segments [6,7]. Mutations such as *Bicaudal-D* (*Bic-D*), *ik2*, and others that produce a duplicated anterior focus of *osk* mRNA also produce bicaudal embryos [8–10]. Conversely, embryos from females carrying hypomorphic loss-of-function mutations of *osk* lack posterior segmentation and pole cells [11]. Mutations in a number of other genes can produce a similar phenotype, and these are collectively known as posterior-group genes [12]. Some of these genes (for example *cappuccino*, *chickadee*, *spire* and *staufen* (*stau*)) are required for posterior localization of *osk*. A failure to deploy *osk* produces the posterior-group phenotype in these mutants [13,14]. Other posterior-group genes (for example *vasa* (*vas*), *tudor*, *nanos* (*nos*), and *aubergine* (*aub*)), produce mRNAs and/or proteins that also accumulate in pole plasm and operate downstream of *osk* [15–17].

osk translation is under elaborate temporal and spatial regulation, ensuring that Osk protein becomes abundant only in the posterior pole plasm and not before stage 9 of oogenesis [18,19]. A key repressor of *osk* translation prior to that stage and outside the pole plasm is Bruno1 (Bru1), which interacts with binding sites called Bru1 response elements (BREs) in the *osk* 3' UTR. Mutations affecting the BREs result in premature and excessive Osk expression [18–20]. Two mechanisms have been proposed for Bru1-mediated repression of *osk* translation. In the first, Bru1 recruits Cup, which inhibits assembly of an active cap-binding complex by competitively inhibiting eIF4G for binding to eIF4E [21]. The second mechanism involves oligomerization of *osk* mRNA into large ribonucleoprotein particles (RNPs) that are inaccessible to the translational machinery [22–24]. These mechanisms may be connected, in that physically concentrating *osk* mRNA molecules in RNPs can enable regulation in *trans* through inter-molecular interactions. For instance, Bru1 bound to the 3' end of one *osk* mRNA molecule could recruit Cup to eIF4E bound to the 5' cap structure of another *osk* mRNA molecule, thus repressing its translation [25,26]. Importantly, *osk* translation and *osk* mRNA localization are tightly coupled. In nonsense *osk* alleles or when 3' UTR elements required for translational activation are mutated, *osk* mRNA localizes transiently to the pole plasm but its accumulation is not maintained [9,27,28].

While several proteins have been implicated in activating *osk* translation in the pole plasm [14,29,30], a comprehensive picture of how this is achieved has not yet emerged. For instance, it has been proposed that activation of *osk* translation involves inhibition of Bru1 [24]. Related to this, a BRE-containing region in the distal part of the *osk* 3' UTR (BRE-C) functions in repression as well as in activation [25]. Nevertheless, the mechanism underlying the dual function of this element has not yet been solved.

Large-scale *in situ* hybridization screens have identified many other mRNAs that localize to the pole plasm [3,31], and some of the corresponding genes could potentially be involved in *osk* regulation. To search for new posterior-group genes, we previously expressed shRNAs targeting 51 different mRNAs that accumulate in the pole plasm to determine if doing so produced defects in posterior patterning or pole cell formation. We observed that a substantial proportion of embryos produced by *Makorin 1* (*Mkrn1*) knockdown females showed a posterior-group phenotype [32]. Makorin proteins are conserved in plants, fungi, and animals, and contain a RING-domain as well as one or more C₃H-type zinc fingers (ZnF) [33]. The role of Makorin proteins is somewhat enigmatic despite their widespread evolutionary conservation. Mammalian MKRN1 has been identified as an E3 ubiquitin ligase that promotes degradation of target proteins [34–36], but proteomic analysis does not support an association with proteasome components [37,38]. Furthermore MKRN1's shorter isoform stimulates translation in rat forebrain neurons but the mechanism is currently unknown [39].

Here, we analyzed the function of Mkrn1 during oogenesis and early embryogenesis. We generated several alleles that alter different domains of the *Mkrn1* coding sequence. Using these mutants, we found that Mkrn1 is required for accumulation of Osk protein at the posterior pole of the oocyte. We also show that Mkrn1 is not required for *osk* mRNA localization, but essential for its translation. Furthermore, we present evidence that Mkrn1 directly binds to the *osk* 3' UTR via its N-terminal zinc finger domain. Using *Drosophila* S2R+ cells we further found that binding of Mkrn1 to *osk* partially overlaps with the BRE-C domain, adjacent to an A-rich region that recruits pAbp to the *osk* 3' UTR [40]. Moreover, the association between Mkrn1 and *osk* mRNA is stabilized by the physical association with pAbp. Strikingly, depletion of *Mkrn1* results in an increased level of Bru1 binding to *osk* 3' UTR and reduction of *bru1* gene dosage partially rescues *Mkrn1* mutant phenotypes. Based on these data we propose that Mkrn1 competes with Bru1 for *osk* mRNA binding, thus positively regulating *osk* translation and explaining the specific role of BRE-C in translational activation.

Results

The *Drosophila* genome includes four *Makorin*-related genes

In many organisms, up to four distinct genes encoding members of the *Makorin* family exist, but only one such gene, *Mkrn1*, has been annotated in *Drosophila*. To investigate whether flies are unusual in this regard, we searched for sequences similar to human MKRN1. This analysis uncovered four *Drosophila* genes, *Mkrn1*, CG5334, CG5347, and CG12477, with substantial similarity to MKRN1 (S1A Fig). All four predicted polypeptides from these genes contain a region of approximately 130 amino acids that is highly conserved and contains a RING-domain as well as C₃H-type zinc fingers (ZnF). The proteins are otherwise more divergent from one another, with the exception that all but CG12477 contain a ZnF domain near the amino-terminus.

To analyze the differences in their functionalities, we first determined the expression profile of all four *Makorin* genes during development. *Mkrn1* mRNA is expressed at detectable levels at all developmental stages (Fig 1A) and clearly peaks in early (0–2.5 h) embryos and ovaries. In contrast, expression of the other three *Makorin* genes is undetectable during early

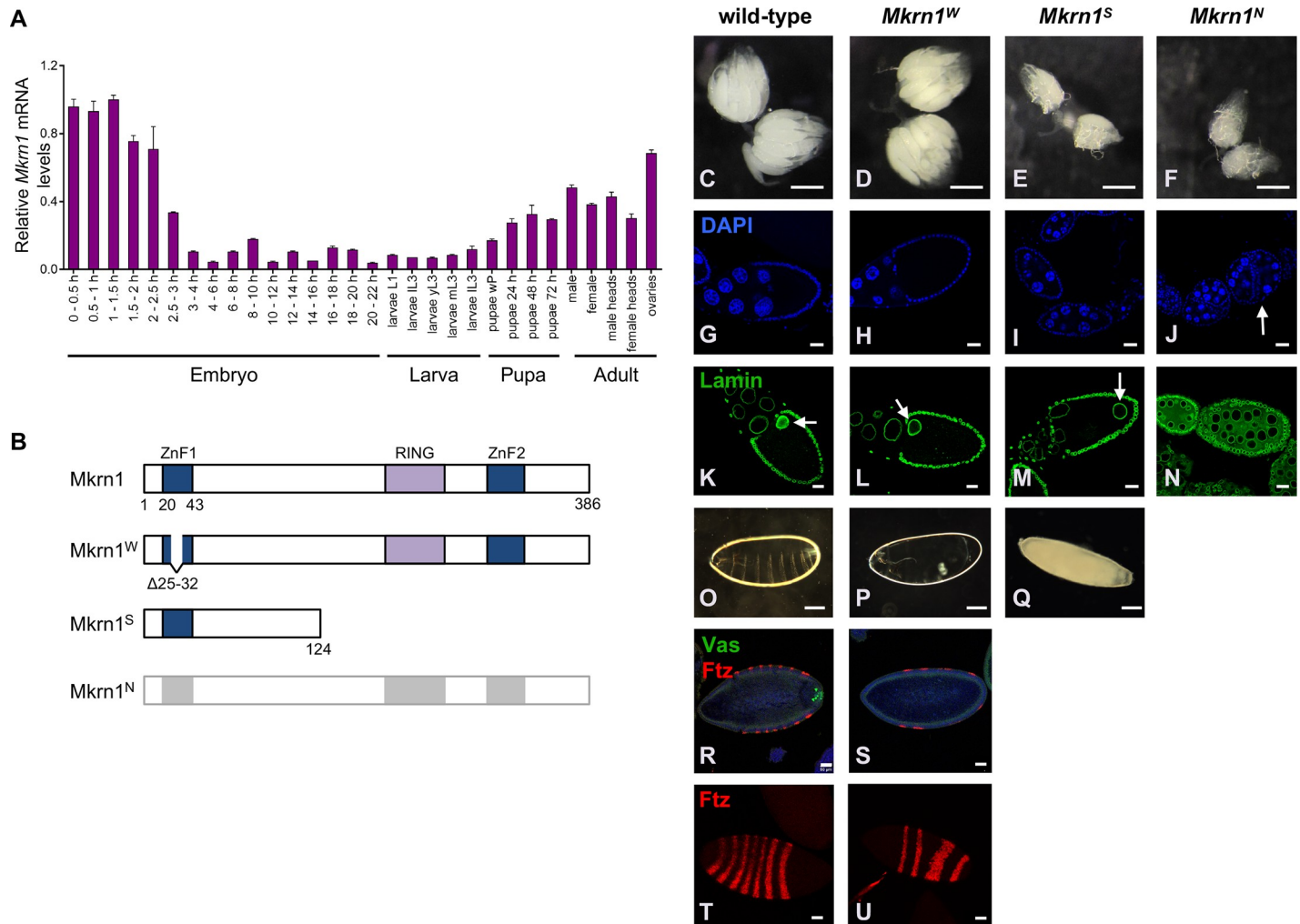


Fig 1. *Mkrn1* alteration affects ovarian development. (A) Relative *Mkrn1* mRNA levels (normalized to *RpL15* mRNA) at various stages of development, measured by quantitative RT-PCR. Error bars depict Stdev, n = 3. (B) Schematic diagram of the proteins encoded by the *Mkrn1* alleles used to analyze its function *in vivo*. *Mkrn1^N* is a null allele and produces no protein. (C-F) Bright-field micrographs of entire ovaries from wild-type and *Mkrn1* mutant flies. Note the reduced size of *Mkrn1^S* and *Mkrn1^N* ovaries. Scale bars, 500 μ m. (G-J) Individual egg chambers stained with the DNA marker DAPI. Fewer stage 10 and older egg chambers are present in *Mkrn1^S* and no late stage egg chambers are present in *Mkrn1^N* ovaries. Abscission defects resulting from inappropriate follicle cell migration are frequently observed in *Mkrn1^N* ovaries (J, arrow). Scale bars, 20 μ m. (K-N) Individual egg chambers stained with α -Lamin to highlight nuclear membranes. Scale bars, 20 μ m. (M) The oocyte nucleus (marked with an arrow in K, L, and M) remains at the posterior of *Mkrn1^S* oocytes. (N) Some *Mkrn1^N* egg chambers have 16 germline cells whose nuclei are all of similar size, suggesting a defect in oocyte differentiation. Note also irregularities in the follicle cell monolayer in the *Mkrn1^N* egg chamber. (O-Q) Dark-field photographs of eggs and embryos produced by wild-type and *Mkrn1* mutants. Scale bars, 100 μ m. (P) Most embryos produced by *Mkrn1^W* females have a posterior-group phenotype. (Q) Eggs produced by *Mkrn1^S* females lack dorsal appendages and do not support embryonic development. (R, S) Immunostaining with α -Ftz (red) and α -Vas (green) reveals segmentation defects and the absence of pole cells in *Mkrn1^W* embryos. Scale bars, 50 μ m. (T, U) Surface images of embryos immunostained with α -Ftz (red) to better illustrate segmentation defects in *Mkrn1^W* embryos. Scale bars, 50 μ m.

<https://doi.org/10.1371/journal.pgen.1008581.g001>

development but peaks in pupae and adult males (S1B Fig). From these results, we conclude that *Mkrn1* is the gene of the family most predominantly expressed in ovaries and early embryos and suggest that the three other genes could be specifically expressed in testes.

Mkrn1 mutants reveal essential roles in oogenesis and embryogenesis

To elucidate the role of *Mkrn1*, we used CRISPR/Cas9 to produce three different mutant alleles: *Mkrn1^N*, a complete deletion of the coding sequence, *Mkrn1^S*, a frameshift mutation that is predicted to produce a C-terminally truncated protein of 124 amino acids, including

Table 1. Expression of tagged *Mkrn1* from transgenes rescues oogenesis and viability to embryos produced by *Mkrn1* mutant females.

Genotype	Eggs laid	Hatched	Unhatched	Hatching %
<i>nos>Gal4/CyO; Mkrn1^W/Mkrn1^W</i>	1222	40	1182	3.3
<i>FLAG-Mkrn1/nos>Gal4; Mkrn1^W/Mkrn1^W</i>	2120	1690	430	79.7
<i>Venus-Mkrn1/nos>Gal4; Mkrn1^W/Mkrn1^W</i>	1180	895	285	75.8
<i>nos>Gal4/CyO; Mkrn1^S/Mkrn1^S</i>	12	0	12	0.0
<i>FLAG-Mkrn1/nos>Gal4; Mkrn1^S/Mkrn1^S</i>	750	465	285	62.0
<i>Venus-Mkrn1/nos>Gal4; Mkrn1^S/Mkrn1^S</i>	1320	1065	255	80.0
<i>nos>Gal4/CyO; Mkrn1^N/Mkrn1^N</i>	0	0	0	0.0
<i>FLAG-Mkrn1/nos>Gal4; Mkrn1^N/Mkrn1^N</i>	1030	760	270	73.8
<i>Venus-Mkrn1/nos>Gal4; Mkrn1^N/Mkrn1^N</i>	1255	1080	175	86.1

<https://doi.org/10.1371/journal.pgen.1008581.t001>

only ZnF1 among conserved domains, and *Mkrn1^W*, a small in-frame deletion that disrupts only the ZnF1 domain (Fig 1B). In the strong *Mkrn1* mutants (*Mkrn1^S* and *Mkrn1^N*), most egg chambers cease development at or before stage 10 (Fig 1C–1J). The nuclei of *Mkrn1^S* oocytes that progress as far as stage 9 or later remain at the posterior, failing to migrate to the antero-dorsal corner (Fig 1M). The very few eggs laid by *Mkrn1^S* females have no dorsal appendages and do not develop (Fig 1Q). *Mkrn1^N* egg chambers do not progress as far as stage 9 and showed variable defects in early oogenesis including failure of oocyte differentiation (Fig 1N) and inappropriate follicle cell migration (Fig 1J and 1N). On the other hand, ovaries of females homozygous for *Mkrn1^W* have a similar morphology to wild-type (Fig 1C and 1D). *Mkrn1^W* mutant ovaries completed oogenesis and produced fertilizable eggs in similar numbers as wild-type controls (Fig 1G, 1H, 1K and 1L, Table 1). To examine the role of *Mkrn1* in embryonic patterning, we compared cuticle preparations of wild-type and *Mkrn1^W* embryos (Fig 1O and 1P). We found that most *Mkrn1^W* embryos lack posterior segments, a phenotype similar to *osk* mutants and to what we previously observed at lower frequency from females expressing shRNA targeting *Mkrn1* [32]. To investigate this more closely, we stained wild-type and *Mkrn1^W* embryos for Fushi tarazu (Ftz) and Vas proteins. In wild-type blastoderm-stage embryos, Ftz is expressed in seven stripes along the anterior-posterior axis, while in posterior-group embryos the number of Ftz stripes is usually reduced to four (Fig 1R and 1T, [41]). At blastoderm stage in wild-type embryos, Vas-positive pole cells are clustered at the posterior pole [16] (Fig 1R). Consistent with a posterior-group phenotype, we observed four Ftz stripes in 65% of *Mkrn1^W* embryos (30/46) (Fig 1S and 1U). Most of the remaining embryos had even fewer Ftz stripes with an additional broad domain of Ftz expression. In addition, 95% of *Mkrn1^W* embryos (63/66) showed no pole cells by Vas staining (Fig 1S). The posterior patterning defects result in lethality for most (97%) *Mkrn1^W* embryos. However, the small number of *Mkrn1^W* embryos that hatch into viable larvae (40/1222, 3.3%, Table 1) can complete development to adulthood.

Mkrn1 accumulates in the pole plasm during oogenesis

To examine the distribution of Mkrn1 in the germline, we expressed transgenic Venus- and FLAG-tagged Mkrn1 using a *nos>GAL4* driver. Since *Mkrn1* females could be rescued to fertility by germline specific expression of these transgenes (Table 1), we concluded that these tagged transgenes are functional, and thus inferred that their localization should reflect the endogenous one. When expressed in ovaries, Venus- or FLAG-tagged Mkrn1 (subsequently called Mkrn1) becomes detectable in a uniform distribution in germline cells from early oogenesis. We observed a mild accumulation of Mkrn1 in cytoplasmic particles resembling

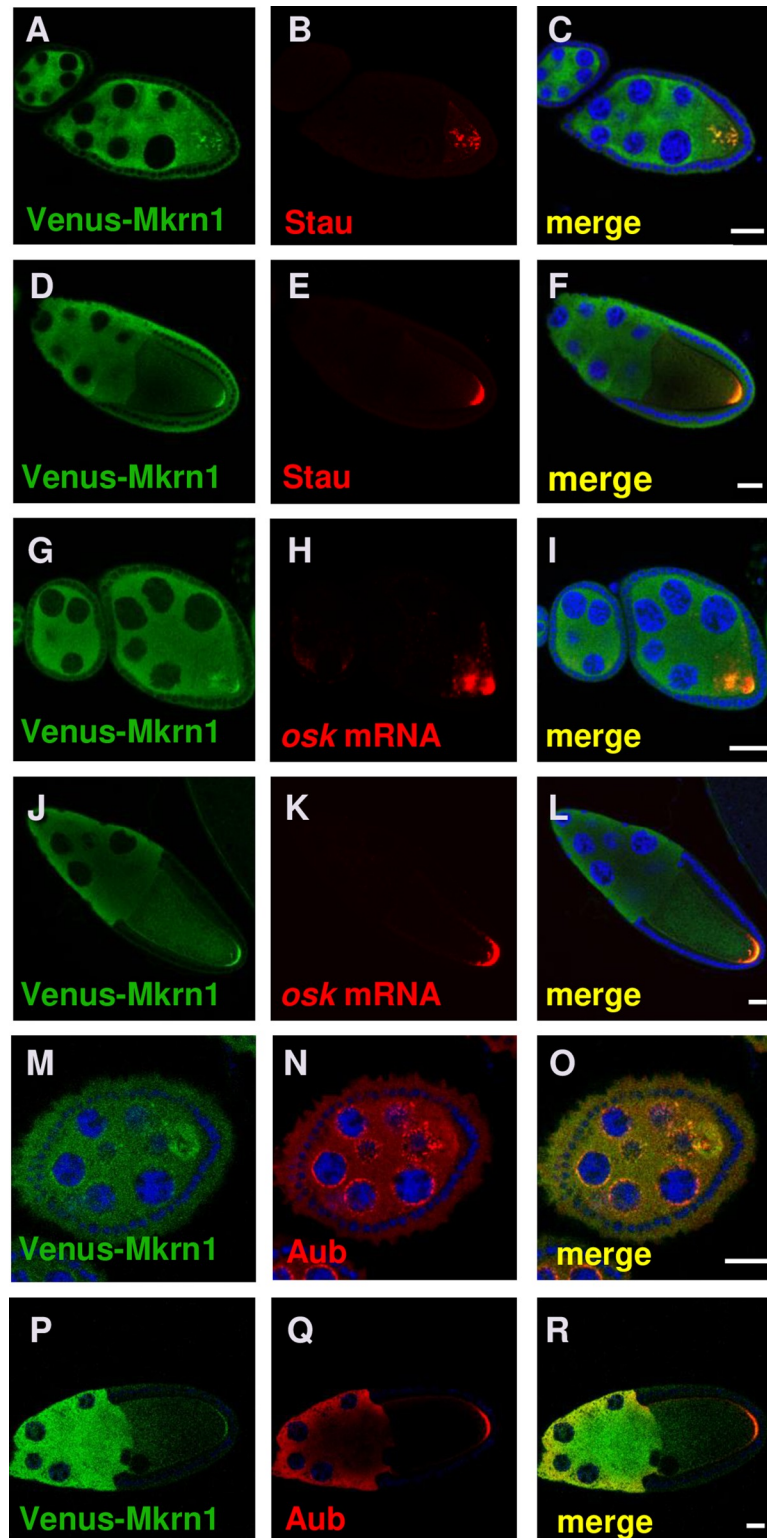


Fig 2. Mkrn1 accumulates in pole plasm. (A-C) The three panels show the same egg chambers stained for (A) Venus-Mkrn1, (B) Stau, and a (C) merged image. Scale bars, 25 μ m. Venus-Mkrn1 expression was driven by *nos*>Gal4. Colocalization of Venus-Mkrn1 and Stau can be observed in particles that have not yet accumulated at the posterior of the early stage 8 oocyte. (D-F) The three panels show the same stage 10 egg chamber stained for (D) Venus-Mkrn1, (E) Stau and (F) a merged image. Scale bars, 25 μ m. There is extensive colocalization of Venus-Mkrn1 and Stau in the

posterior pole plasm of the oocyte. (G-I) The three panels show the same egg chambers stained for (G) Venus-Mkrn1, (H) *osk* mRNA, and (I) a merged image. Scale bars, 25 μ m. Colocalization of Venus-Mkrn1 and *osk* can be observed in an early stage 8 oocyte where *osk* has not yet fully localized at the posterior of the oocyte. (J-L) The three panels show the same stage 10 egg chamber stained for (J) Venus-Mkrn1, (K) *osk* mRNA and (L) a merged image. Scale bars, 25 μ m. There is extensive colocalization of Venus-Mkrn1 and *osk* mRNA in the posterior pole plasm of the oocyte. (M-O) The three panels show the same egg chambers stained for (M) Venus-Mkrn1, (N) Aub, and a (O) merged image. Scale bars, 5 μ m. Colocalization of Venus-Mkrn1 and Aub can be observed at the nuage surrounding the nurse cell nuclei (P-R). The three panels show the same egg chambers stained for (P) Venus-Mkrn1, (Q) Aub, and a (R) merged image. Scale bars, 20 μ m. There is extensive colocalization of Venus-Mkrn1 and Aub in the posterior pole plasm of the oocyte.

<https://doi.org/10.1371/journal.pgen.1008581.g002>

nuage at the outer surface of nurse cell nuclear membranes and in the early oocyte (Fig 2A, 2G and 2M). In later egg chambers, Mkrn1 remains abundant in nurse cells and is tightly localized in the pole plasm in the oocyte (Fig 2D, 2J and 2P). Next, we conducted double labeling experiments in wild-type ovaries to determine the degree of colocalization between Mkrn1 and known pole plasm components. In both, stage 8 and stage 10 oocytes, Mkrn1 co-localizes extensively with Stau (Fig 2A–2F), *osk* mRNA (Fig 2G–2L), Osk protein (S2A–S2F Fig), Vas (S2G–S2L Fig) and Aub (Fig 2M–2R). This close association between Mkrn1 and many important pole plasm components suggests that Mkrn1 is an integral component of pole plasm.

To determine whether Mkrn1 depends on the pole plasm assembly pathway for its posterior localization, we expressed the tagged *Mkrn1* transgenes in *osk* (*osk*^{54/Df}) and *vas* (*vas*^{PH165/vas¹}) mutant backgrounds. We found that loss of *osk* abolished Mkrn1 localization (S3A Fig). In contrast, Mkrn1 localized normally to the posterior in *vas* mutant oocytes (S3B Fig), placing Mkrn1 between *osk* and Vas in the pole plasm assembly pathway.

To obtain insights into the link between Mkrn1 and pole cell determination, we collected embryos from females trans-heterozygous for a *Mkrn1* allele and for either a *vas* or *osk* allele. Next, we compared the number of pole cells with single heterozygous controls. When heterozygous, *Mkrn1*^W or *Mkrn1*^S had little effect on pole cell number. However, either allele reduced the number of pole cells produced by *vas*¹ heterozygotes, and further by *osk*⁵⁴ heterozygotes (S4 Fig). These data support a genetic interaction between *Mkrn1* and genes involved in embryonic patterning and pole cell specification.

Mkrn1 ensures correct deployment of specific mRNAs and proteins involved in embryonic patterning

To address whether *Mkrn1* mutations may affect the distribution of proteins involved in embryonic patterning, we performed immunostaining experiments. We found a striking reduction in posterior accumulation of Osk in oocytes from all *Mkrn1* alleles (Fig 3A–3D). For Stau, we observed weaker and more diffuse posterior localization in *Mkrn1*^W, as compared to wild-type (Fig 3E and 3F) and no localized protein in *Mkrn1*^S and *Mkrn1*^N (Fig 3G and 3H). On the other hand, Grk localized normally to the antero-dorsal corner of *Mkrn1*^W oocytes (Fig 3I and 3J). In *Mkrn1*^S, Grk was observed at reduced levels associated at the posterior with the mislocalized oocyte nucleus (Fig 3K) and diffusely distributed at a very low level in *Mkrn1*^N (Fig 3L). Posterior localization of Aub and Vas was lost in oocytes of all *Mkrn1* mutant alleles (Fig 3M–3T). Finally, Orb localization was unaffected in *Mkrn1*^W (Fig 3U and 3V), but was concentrated at the posterior in *Mkrn1*^S (Fig 3W). Many *Mkrn1*^N egg chambers included a single Orb-positive cell (Fig 3X), indicating that, in these cases, oocyte differentiation had taken place. Importantly, normal accumulation of all proteins could be restored by *nos*>GAL4 driven expression of a tagged *Mkrn1* transgene (S5 Fig), confirming the specificity of the *Mkrn1* phenotypes.

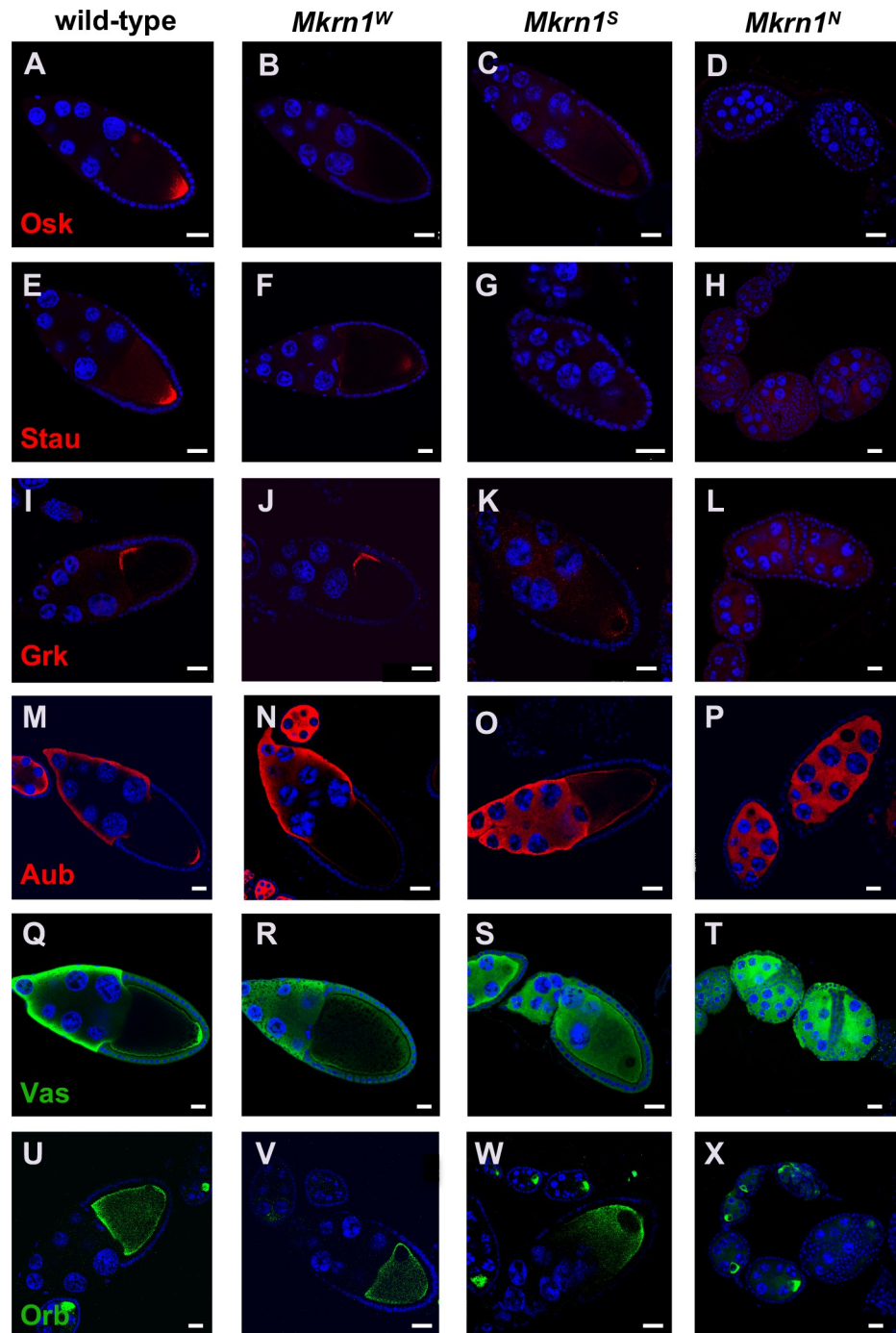


Fig 3. *Mkrn1* mutations affect accumulation of proteins involved in axis patterning. (A-D) Posterior accumulation of Osk is greatly reduced in stage 10 *Mkrn1^W* and *Mkrn1^S* oocytes as compared with wild-type. Osk is nearly undetectable in *Mkrn1^N* egg chambers. Scale bars, 25 μ m. (E-H) Posterior accumulation of Stau is greatly reduced in stage 10 *Mkrn1^W* and *Mkrn1^S* oocytes as compared with wild-type. Stau is nearly undetectable in *Mkrn1^N* egg chambers. Scale bars, 25 μ m. (I-L) Anterodorsal accumulation of Grk is normal in stage 10 *Mkrn1^W* oocytes. Grk remains associated with the oocyte nucleus and is mislocalized to the posterior in stage 10 *Mkrn1^S* oocytes. Grk is present at uniformly low levels or undetectable levels in all germ cells in *Mkrn1^N* egg chambers. Scale bars, (I-K) 20 μ m, (L) 25 μ m. (M-P) Posterior accumulation of Aub is greatly reduced in stage 10 *Mkrn1^W* and *Mkrn1^S* oocytes as compared with wild-type. Aub is present at uniform levels in all germ cells in *Mkrn1^N* egg chambers. Scale bars, 20 μ m. (Q-T) Posterior accumulation of Vas is greatly reduced in stage 10 *Mkrn1^W* and *Mkrn1^S* oocytes as compared with wild-type. Vas is present at uniform levels in all germ cells in *Mkrn1^N* egg chambers. Scale bars, 25 μ m. (U-X)

Accumulation of Orb is similar in wild-type and *Mkrn1^W* oocytes, but Orb is more concentrated in the posterior of *Mkrn1^S* oocytes. In early-stage *Mkrn1^N* egg chambers there is usually a single Orb-positive cell, indicating that some steps toward oocyte differentiation are able to take place. Scale bars, (U-W) 20 μm, (X) 25 μm.

<https://doi.org/10.1371/journal.pgen.1008581.g003>

Mkrn1^W oocytes transiently accumulate *osk* mRNA at the posterior pole but do not produce Osk protein

To investigate whether the primary effect of *Mkrn1^W* on Osk deployment occurred at the level of RNA localization or translation, we examined more closely the effects of *Mkrn1^W* on *osk* expression. Therefore, we performed *in situ* hybridization for *osk* mRNA and immunostaining for Osk protein on the same samples (Fig 4A). In stage 7 egg chambers, *osk* mRNA accumulation is robust in both wild-type and *Mkrn1^W* oocytes. Faint expression of Osk protein is occasionally visible in wild-type stage 7 oocytes but never in similarly staged *Mkrn1^W* oocytes. This difference becomes more pronounced in stages 9 and 10A. While 95% (41/43) of stage 9-10A *Mkrn1^W* oocytes show posterior accumulation of *osk* mRNA, only 7% (3/43) of *Mkrn1^W* oocytes show even a faint posterior signal for Osk protein. All (20/20) similarly-staged wild-type oocytes show strong posterior accumulation of both *osk* mRNA and Osk protein (Fig 4A). Subsequently, posterior accumulation of *osk* mRNA is lost in *Mkrn1^W* oocytes. In 88% of stage 10B *Mkrn1^W* oocytes (30/34), *osk* mRNA remains in a tight focus, but is no longer anchored at

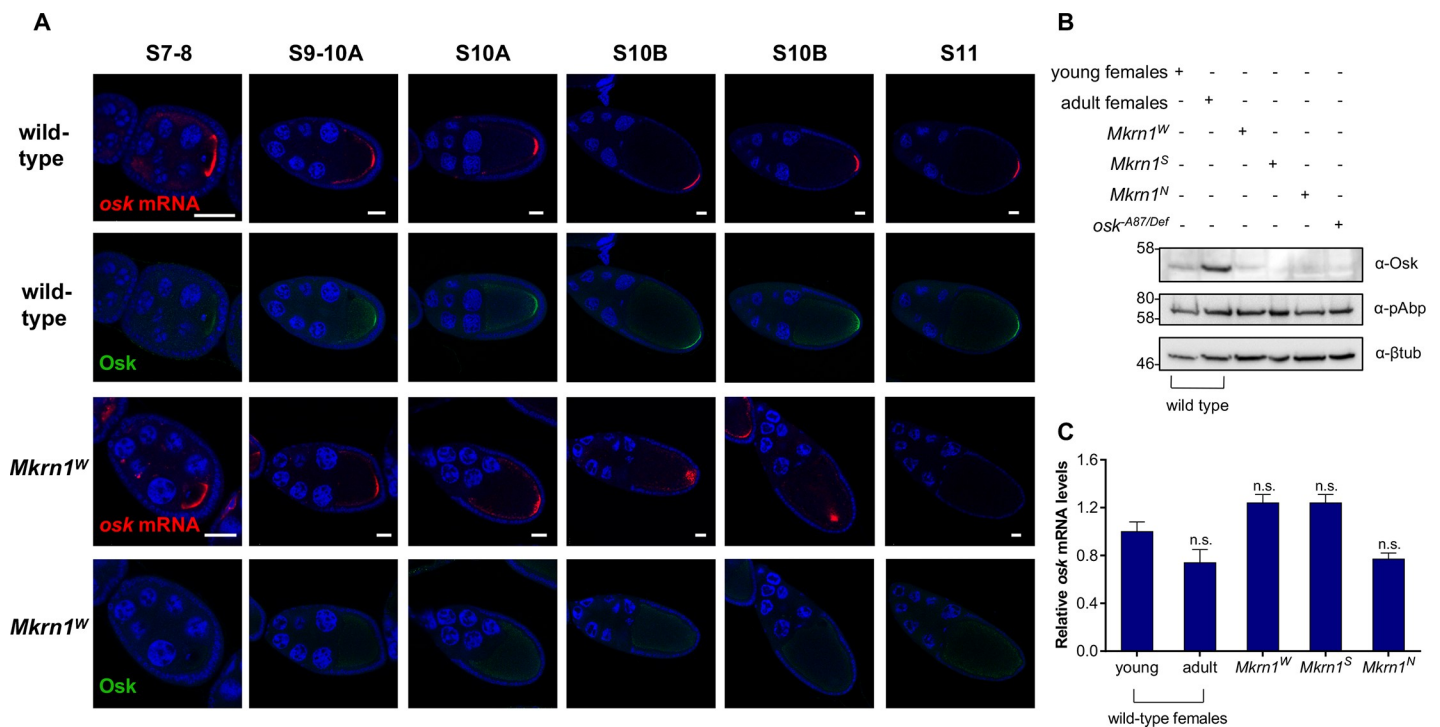


Fig 4. Translation of *osk* mRNA is impaired in *Mkrn1^W* ovaries. (A) Fluorescent *in situ* hybridization for *osk* mRNA (red) with co-immunostaining for Osk protein (green) in wild-type and *Mkrn1^W* egg chambers. For each genotype and in each column the top and bottom images are of the same egg chamber. In wild-type oocytes posterior accumulation of *osk* mRNA and Osk protein is robust and stable from stage 9 onward. In *Mkrn1^W* oocytes accumulation of *osk* mRNA resembles the wild-type pattern through stage 10A but is not maintained, while Osk protein is rarely detectable at the oocyte posterior at any stage. Scale bars, 25 μm. (B) Western blot analysis from ovary lysates of various genotypes stained for Osk, pAbp and β-tubulin. Osk protein levels are greatly reduced in all *Mkrn1* mutant alleles. 1 day-old young females have not yet completed oogenesis and were used as a control for *Mkrn1^S* and *Mkrn1^N* ovaries which also lack late-stage egg chambers, where Osk is most abundant. (C) RT-qPCR experiments measuring ovarian *osk* mRNA levels (normalized to *Rpl15* mRNA) in the same genotypes as (B). mRNA levels of ovaries from adult females were compared to *Mkrn1^W* ovaries. For *Mkrn1^S* and *Mkrn1^N* ovaries, mRNA levels of 1 day-old young ovaries was used as normalization. Error bars depict Stdev, n = 2.

<https://doi.org/10.1371/journal.pgen.1008581.g004>

the posterior pole (Fig 4A). *osk* translation remains repressed with only 6% of stage 10B *Mkrn1^W* oocytes (2/34) having detectable posterior Osk. In later *Mkrn1^W* oocytes, neither *osk* mRNA nor Osk protein is detectable at the posterior. We conclude from these experiments that *Mkrn1* is not directly required for the localization of *osk* mRNA at the posterior pole but is necessary for its translation. Consistent with previous observations in other conditions that abrogate Osk anchoring or translation [9,27,28,42], posterior accumulation of *osk* mRNA is not maintained in *Mkrn1^W* oocytes because of their failure to accumulate localized Osk protein. To confirm these results, we compared Osk protein levels by western blot analysis and *osk* mRNA levels by quantitative PCR (qPCR). Consistent with our immunostaining experiments, we observed a pronounced reduction in Osk protein (Fig 4B), but only minor positive or negative effects on *osk* mRNA depending on the particular *Mkrn1* allele (Fig 4C).

***Mkrn1* mutants affect localization of other maternal mRNAs**

We further used fluorescent *in situ* hybridization to investigate the distribution of several other mRNAs involved in patterning in *Mkrn1* mutants. Consistent with what we observed for Grk protein, localization of *grk* mRNA was similar to wild-type in *Mkrn1^W*, but *grk* mRNA remained at the posterior in *Mkrn1^S* oocytes (S6A–S6C Fig). Posterior accumulation of *osk*, *nos* and *polar granule component* (*pgc*) mRNAs was also lost in *Mkrn1^W* embryos (S6D–S6I Fig).

***Mkrn1* associates with factors involved in *osk* mRNA regulation**

To gain further insights into the molecular pathways underlying *Mkrn1* function we sought to identify potential cofactors. For this purpose, we expressed Myc-tagged *Mkrn1* in *Drosophila* S2R+ cultured cells and carried out immunoprecipitation (IP) experiments followed by mass spectrometry analysis. We also repeated this experiment using a version of *Mkrn1* carrying a point mutation in the RING domain (*Mkrn1^{RING}*), as we noticed that this construct was expressed at a higher level compared to the wildtype one, which appears to be unstable after transfection in cells (S7A and S7B Fig). Similar stability characteristics have been reported for mammalian MKRN1 [34]. Numerous RNA-binding proteins were enriched after IP (S7C and S7D Fig). Among those, several have been already linked to *osk* mRNA localization and translation [21,40,43–45]. To validate these interactions, we performed co-IP experiments in S2R+ cells between *Mkrn1^{RING}* and various interaction partners in the presence or absence of RNase T1. Using this approach, we could confirm the interaction of *Mkrn1^{RING}* with poly(A) binding protein (pAbp), IGF-II mRNA-binding protein (Imp), eukaryotic initiation factor 4G (eIF4G), Squid (Sqd) and maternal expression at 31B (Me31B) (S8A–S8E Fig). All of these interactions persisted upon RNase treatment, suggesting they are direct. We can however not exclude the possibility that the poly(A) tail, which is not affected by treatment with RNase T1, mediates these interactions. Interestingly, several of the identified proteins have already been shown to interact with each other [43,44,46–48]. We also confirmed that interactions between FLAG-tagged *Mkrn1* and pAbp as well as eIF4G also occur in ovaries (Fig 5A and S8F Fig).

Furthermore, we found that the stability of *Mkrn1* itself was enhanced upon co-transfection of pAbp in S2R+ cells (Fig 5B). Mammalian MKRN1 contains a PCI/PINT associated module 2 (PAM2) motif, that is present in several pAbp binding proteins and is required in MKRN1 for binding to PABP [39,49]. We identified a similar motif in *Drosophila* *Mkrn1* (Fig 5C), but with one variation compared to human (V instead of E at position 9) that likely explains why this PAM2 motif was not recognized previously. To address the functionality of this motif we repeated the co-IPs, and found that when this domain was mutated (*Mkrn1^{PAM2}*, Fig 5C), the interaction between *Mkrn1* and pAbp was compromised in S2R+ cells (Fig 5D). Based on

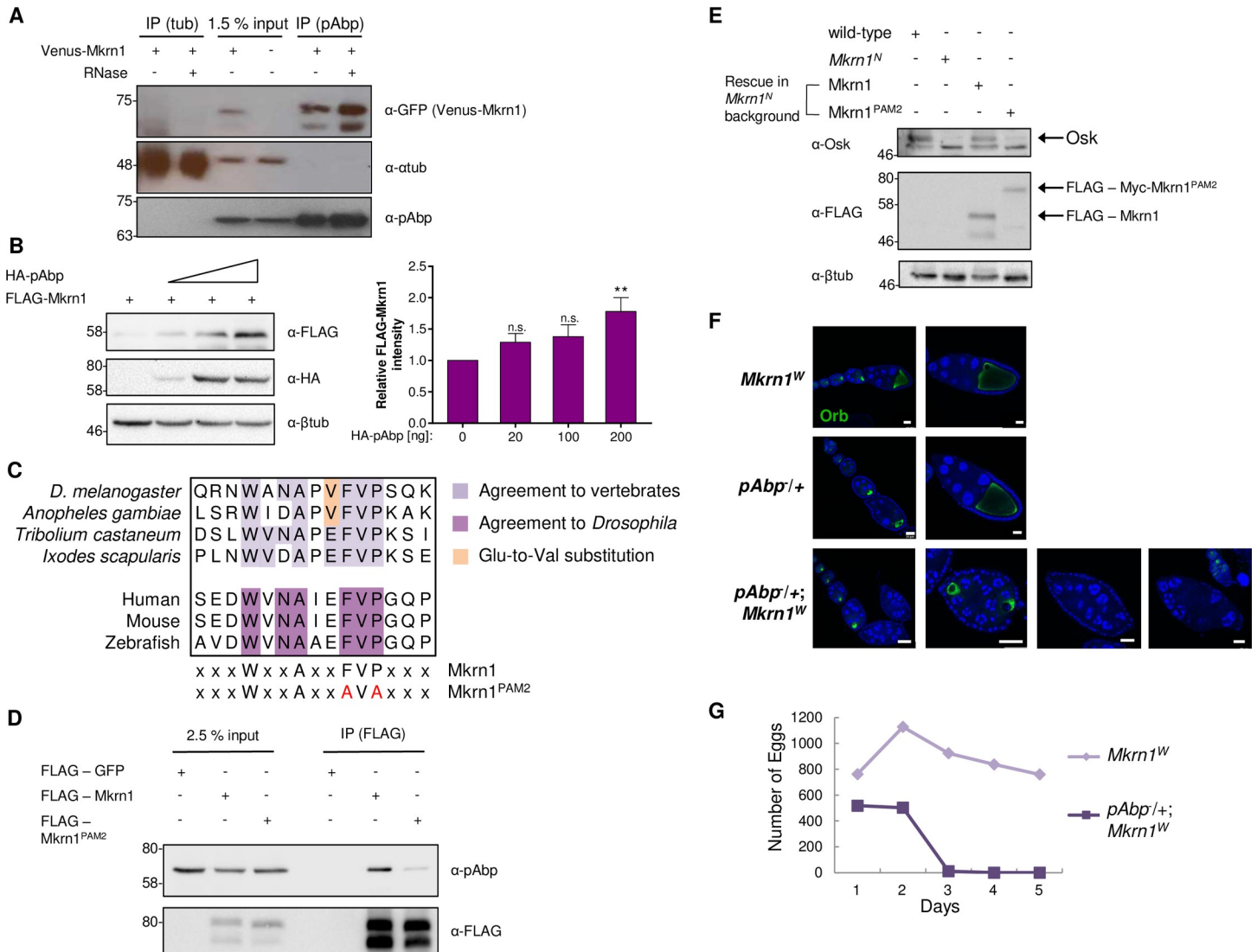


Fig 5. Mkrn1 interacts strongly with the poly(A) binding protein. (A) Western blot analysis of co-IP experiments between Venus-Mkrn1 and pAbp. α -Tubulin (lanes 1, 2) and ovaries lacking the Venus-Mkrn1 transgene (lane 4) were used as negative controls. (B) Co-expression of pAbp stabilizes Mkrn1. FLAG-Mkrn1 was co-transfected with increasing levels of HA-pAbp in S2R+ cells. Left: Proteins were examined using immunoblotting. Right: Intensities of FLAG-Mkrn1 levels were quantified and normalized to intensities of β -tubulin. The relative intensity was normalized to *Mkrn1* mRNA levels (normalized to *RpL15* mRNA) analyzed by RT-qPCR. Error bars depict SEM, n = 9. (C) PAM2 motif alignment in different species. Comparison between *Drosophila* and human PAM2 revealed a Glu to Val substitution (orange) in the consensus sequence. The conserved amino acid sequence to *Drosophila* (dark purple) is indicated below. The PAM2 motif was mutated using two amino acid substitutions at positions 90 and 92 to alanine (F90A and P92A). (D) Immunoblot analysis of co-IP experiments between FLAG-Mkrn1 and pAbp in S2R+ cells. The interaction of pAbp and Mkrn1 is reduced when the PAM2 motif is mutated. (E) Rescue experiments of wild-type or mutant Mkrn1 in *Mkrn1^N* mutants. FLAG-Mkrn1 or FLAG-Myc-Mkrn1^{PAM2} was overexpressed in ovaries using a *nos>Gal4* driver line. Ovarian protein lysates from rescued females were analyzed by immunoblotting together with wild-type and *Mkrn1^N* as controls. While Mkrn1 overexpression could restore Osk protein level to approximately wild-type, Mkrn1^{PAM2} depicted decreased protein levels similar to *Mkrn1^N*. (F) Egg chambers from (top panel) *Mkrn1^W*, (middle panel) *pAbp^{+/+}*, and (bottom panel) *pAbp^{+/+}; Mkrn1^W* females stained with DAPI and immunostained for Orb, an oocyte marker. *pAbp^{+/+}; Mkrn1^W* ovaries show diverse developmental defects. Scale bars, 25 μ m except for the lower left panel, where the scale bar is 50 μ m. (G) Time course of fecundity of *Mkrn1^W* and *pAbp/CyO; Mkrn1^W* females.

<https://doi.org/10.1371/journal.pgen.1008581.g005>

these data, we conclude that Mkrn1 exists in one or several complexes that contain factors involved in the regulation of *osk* mRNA translation, and stably interacts with pAbp via its PAM2 motif. If the interaction of Mkrn1 with pAbp is indeed required for the function of Mkrn1, Mkrn1^{PAM2} should not be able to rescue the *Mkrn1^N* phenotype. Indeed, we found that overexpression of Mkrn1^{PAM2} in *Mkrn1^N* ovaries could not rescue Osk protein levels and

posterior localization compared to wild-type Mkrn1 (Fig 5E and S9B Fig). Moreover, we observed a strong modifier effect between *Mkrn1^W* and *pAbp* mutations; *Mkrn1^W* homozygotes and *pAbp* heterozygotes complete oogenesis, but many egg chambers from *pAbp/+*; *Mkrn1^W* females show severe defects, including supernumerary germ cells, missing or duplicated oocytes, or more extreme dysmorphologies (Fig 5F). These females can produce eggs, but only for the first 2–3 days of life (Fig 5G), and these eggs did not support embryonic development. We thus conclude that the interaction of Mkrn1 with pAbp is essential for its function during oogenesis.

Mkrn1 associates specifically with *osk* mRNA *in vivo*

The effects we observed on *osk* translation in late *Mkrn1* egg chambers prompted us to test whether Mkrn1 can interact with *osk* mRNA. First, to assess whether Mkrn1 can bind to RNA in general, we immunoprecipitated FLAG-Mkrn1 after transfection of S2R+ cells and UV crosslinking. Mkrn1-bound RNA was subsequently labeled, and the protein-RNA complexes were visualized by autoradiography (S10A Fig). While a higher concentration of RNase I (1/50 dilution) resulted in a focused band, a lower concentration (1/5000 dilution) produced a shift of the Mkrn1-RNA complexes, demonstrating the RNA binding ability of *Drosophila* Mkrn1. We next repeated this experiment with various mutations in different Mkrn1 domains (S7A and S10A Fig). While mutations that alter the RING (Mkrn1^{RING}) or the ZnF2 domain (Mkrn1^{ZnF2}) behave as wild-type Mkrn1, deletion of the ZnF1 domain (Mkrn1^{ΔZnF1}) resulted in a reduction of labeled Mkrn1-RNA complexes. These findings demonstrate that *Drosophila* Mkrn1 can bind to RNA and the ZnF1 domain is critical for this binding.

To confirm that Mkrn1 binds *osk* mRNA *in vivo*, we overexpressed either FLAG-tagged wild-type Mkrn1 or Mkrn1^{ΔZnF1} in ovaries and performed RNA IP (RIP) experiments. The enrichment of different mRNAs was analyzed by qPCR using primers that bind to the 3' UTRs of the respective transcripts. Interestingly, we observed that *osk* mRNA was substantially enriched in Mkrn1 IPs, but much less so when using Mkrn1^{ΔZnF1} (Fig 6A and S10B Fig). On the other hand, *bicoid* (*bcd*) and *grk* mRNAs were not detected above background levels in either RIP experiment. This provides evidence that Mkrn1 binds specifically to *osk* mRNA in ovaries and that its ZnF1 domain is important for this interaction.

To determine precisely where Mkrn1 binds to *osk* mRNA, we performed individual nucleotide resolution cross-linking and immunoprecipitation (iCLIP), an unbiased approach to identify RNA-binding sites of a protein of interest [50]. This condition ensured that all Mkrn1 protein-RNA complexes were potentially recoverable in the immunoprecipitations. To this end, we overexpressed FLAG-tagged Mkrn1 in S2R+ cells and performed iCLIP experiments (S10C Fig). Since *osk* is poorly expressed in these cells, we co-transfected a genomic construct of *osk* under the control of an *actin* promoter. We found specific binding sites in a handful of genes, including *osk*, ranking at third position in term of read coverage (S10D Fig), in which Mkrn1 binding sites were located in the distal part of the 3' UTR (Fig 6B). These sites fall just upstream of an A-rich sequence that associates with pAbp [40]. Moreover, the binding site of Mkrn1 partially overlaps with the BRE-C site, which is bound by Bru1 and is required for both repression and activation of *osk* translation [25].

To validate the identified Mkrn1 binding sites, we performed RIP experiments in S2R+ cells using different 3' UTRs fused to the *firefly luciferase* coding sequence. We found that Mkrn1 binds strongly to *osk* 3' UTR but not significantly above background levels to *grk* 3' UTR (S11A Fig). In addition, deletion of the Mkrn1-bound site identified with iCLIP in cells (*osk*^{ΔMkrn1}, deletion of nucleotides 955–978 of *osk* 3' UTR) greatly reduced the interaction of Mkrn1 to *osk* 3' UTR (Fig 6C and S11B Fig).

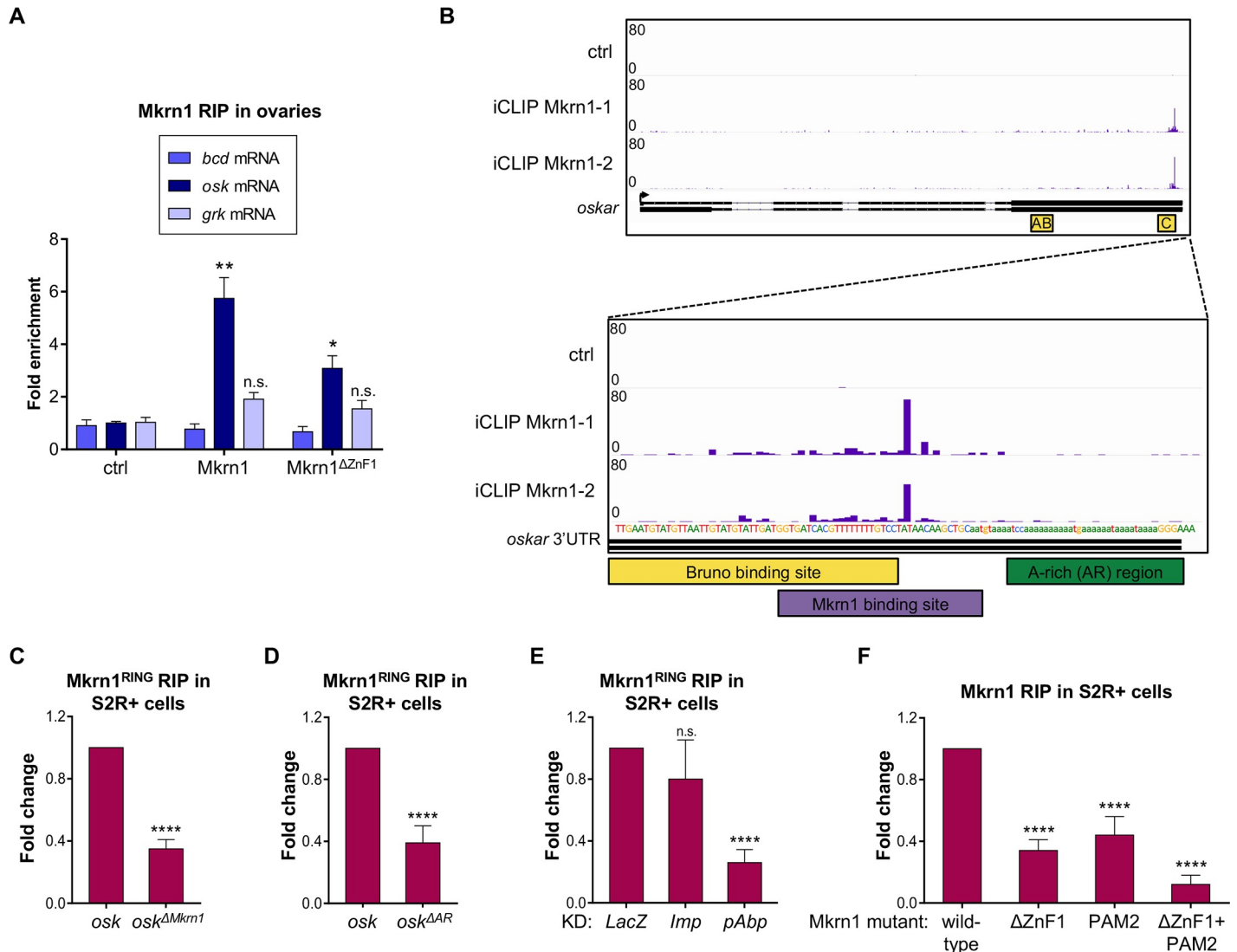


Fig 6. Mkrn1 associates specifically with the 3' UTR of *osk* mRNA. (A) RIP experiment. Either FLAG-tagged Mkrn1 or Mkrn1 Δ ZnF1 was overexpressed in Mkrn1^N ovaries using *nos>GAL4* driver. Enrichment of different transcripts was analyzed by RT-qPCR using primers that bind to the respective 3' UTRs. Fold enrichment is presented relative to the control (*nos>GAL4* driver alone, ctrl). Error bars depict SEM, n = 3. Multiple t-test was used to analyze significant changes compared to control RIP. (B) iCLIP results from S2R+ cells showing specific binding of Mkrn1 to *osk* in a region of the 3' UTR that partially overlaps with the BRE-C site (yellow). The peaks (purple) indicate crosslinking events of Mkrn1 to *osk*. Data of two technical replicates for FLAG-Mkrn1 is shown. The same experiment performed with FLAG-GFP (ctrl) did not show specific peaks. (C) RIP experiments of FLAG-Mkrn1^{RING} in S2R+ cells. Enrichment of *luciferase-osk-3'UTR* transcript was analyzed by RT-qPCR compared to IP experiments with FLAG-GFP. Mkrn1^{RING} binding to *osk* 3' UTR is compromised when introducing a deletion of the Mkrn1 binding site (*osk* Δ Mkrn1, deletion of nucleotides 955–978 of *osk* 3' UTR). Error bars depict SEM, n = 4. (D) Binding of Mkrn1^{RING} to *luciferase-osk-3'UTR* reporter is reduced in S2R+ cells when using a deletion of the A-rich region of *osk* 3' UTR (*osk*^{AAR}, deletion of nucleotides 987–1019 of *osk* 3' UTR). Fold change illustrates the difference of pulled-down *osk*^{AAR} reporter compared to IP with wild-type *osk* 3' UTR. The RIP experiments were normalized to FLAG-tagged GFP. Error bars depict SEM, n = 4. (E) RIP experiments were performed in either control cells or upon depletion of *Imp* or *pAbp*. Enrichment was calculated compared to FLAG-GFP. The relative change in Mkrn1^{RING} binding to *luciferase-osk-3'UTR* reporter in knockdown cells compared to *LacZ*-depleted cells is depicted. Depletion of *pAbp* compromises binding of Mkrn1. Error bars depict SEM, n = 3. (F) RIP experiments showing that FLAG-Mkrn1 binding to *luciferase-osk-3'UTR* is dependent on the ZnF1 domain as well as on the PAM2 motif. Enrichment was analyzed using RT-qPCR and the relative change in binding compared to RIP of FLAG-Mkrn1 is illustrated. RIP experiments were performed in S2R+ cells using FLAG-GFP as control. Error bars depict SEM, n \geq 3.

<https://doi.org/10.1371/journal.pgen.1008581.g006>

As the Mkrn1 binding site in *osk* 3' UTR lies just upstream of the A-rich region (AR), we wondered whether the AR would also have an impact on Mkrn1 binding. To test this possibility, we deleted the AR (*osk*^{AAR}, deletion of nucleotides 987–1019 of *osk* 3' UTR) and examined

Mkrm1 binding in S2R+ cells. We observed a decrease of Mkrm1 binding similar to that observed when deleting the Mkrm1 binding sites (Fig 6D and S11C Fig). Thus, we conclude that the AR enhances Mkrm1 binding to *osk* 3' UTR. As Mkrm1 forms a stable complex with pAbp, our results further suggest that pAbp binding to the AR stabilizes Mkrm1 and therefore enhances its interaction with *osk*. Accordingly, reducing pAbp levels by RNAi, but not the level of Imp, another Mkrm1 interactor, dramatically decreased Mkrm1 association with *osk* mRNA in *Drosophila* cultured cells (Fig 6E, S11D and S11E Fig). Mutation of the PAM2 domain that enables the interaction with pAbp also resulted in reduced binding to *osk* 3' UTR (Fig 6F and S11F Fig). Consistent with these results, mutating both the ZnF1 domain and the PAM2 motif led to almost complete loss of Mkrm1 binding to *osk* 3' UTR in S2R+ cells. Collectively, our results indicate that Mkrm1 binds specifically to the 3' end of *osk* 3' UTR via its ZnF1 domain and this association is further stabilized through the interaction with pAbp.

Mkrm1 competes with Bru1 for binding to *osk* 3' UTR

Our observation that Mkrm1 binds to the *osk* BRE-C region prompted us to test whether Mkrm1 and Bru1 may compete for binding to *osk* 3' UTR. To this end, we first examined whether we can recapitulate Bru1 binding to *osk* mRNA in S2R+ cells. As Bru1 is normally not expressed in this cell type, cells were co-transfected with GFP-tagged Bru1 along with the *luciferase-osk-3'UTR* reporter. RIP experiments confirmed previous findings that Bru1 strongly associates with *osk* 3' UTR (S12A Fig, [18]). We next repeated this experiment upon knockdown of *Mkrm1* mRNA. Strikingly, while the protein level of Bru1 was not affected (S12B Fig), its binding to *osk* 3' UTR was significantly increased in Mkrm1-depleted cells (Fig 7A and S12B–S12D Fig). As pAbp is required to stabilize the interaction of Mkrm1 to *osk* 3' UTR, we wondered whether it is necessary for modulating Bru1 binding as well. Indeed, knockdown of *pAbp* in S2R+ cells resulted in an increased association of Bru1 to *osk* 3' UTR (Fig 7B and S12E Fig).

Next, to assess if these observations made in cultured cells are relevant to Mkrm1 function *in vivo*, we repeated RIP experiments using ovarian extracts. Bru1 binding was assessed using an antibody directed against endogenous Bru1 and its association with *osk* mRNA was subsequently analyzed by qPCR. Similar to S2R+ cells, the interaction of Bru1 with *osk* was significantly increased in *Mkrm1*^W mutant ovaries (Fig 7 and S12F Fig). Thus, we conclude that Mkrm1 restricts Bru1 binding to *osk* 3' UTR and this effect is enhanced by the interaction of Mkrm1 with pAbp.

To further address the relationship between Mkrm1 and Bru1, we examined whether the *Mkrm1*^W mutation affects Bru1 accumulation during oogenesis. In wild-type ovaries, Bru1 is expressed in all germline cells and accumulates to a modest degree in the oocyte during early oogenesis (Fig 7D and 7E, [20]). However, in *Mkrm1*^W ovaries, oocyte accumulation of Bru1 during early stages was much more pronounced (Fig 7F and 7G). As *osk* mRNA accumulates in early oocytes, this result is consistent with Bru1 having an increased binding affinity for *osk* in the absence of Mkrm1, even though Bru1 can also accumulate in the absence of *osk* RNA [51].

If Mkrm1 activates *osk* translation by displacing Bru1, we would predict that lowering *bru1* genetic dosage should suppress the *Mkrm1* phenotype. To test this hypothesis, we used a strong *bru1* allele (*bru1*^{QB}, [20,52]). We found that removing one copy of *bru1* was sufficient to substantially rescue Osk protein level and posterior localization in *Mkrm1*^W female oocytes as analyzed by immunostainings (Fig 7H–7M). Semi-quantitative analysis of Osk-immunostained ovaries confirmed a clear suppression of the *Mkrm1*^W phenotype by one copy of *bru1*^{QB} (Fig 7N) that was further confirmed by immunoblotting (Fig 7O). We also observed a higher

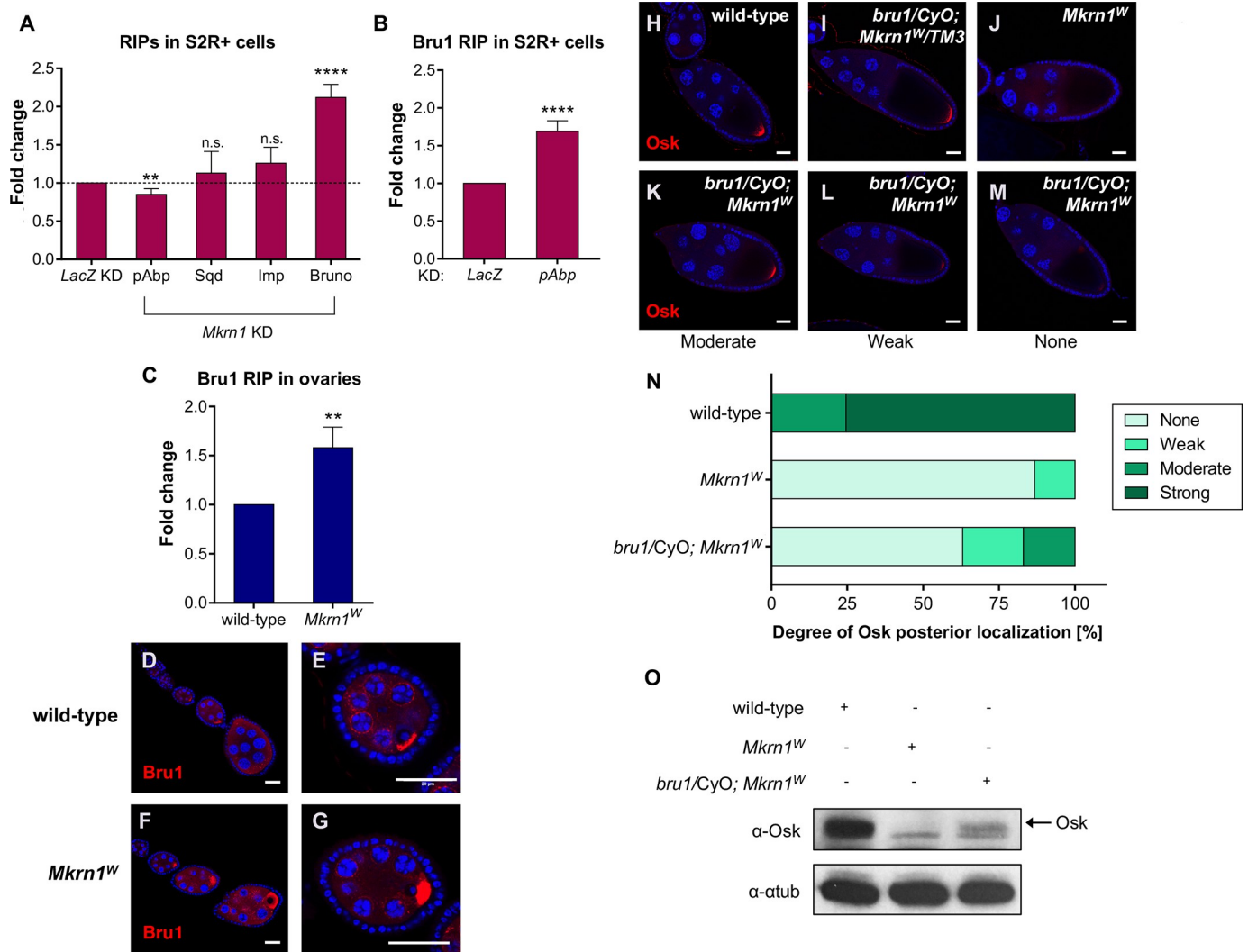


Fig 7. Mkrn1 competes with Bru1 for binding to *osk* mRNA. (A) RIP experiments in either control S2R+ cells, or upon knockdown of *Mkrn1*. Binding of the indicated proteins to the *luciferase-osk*-3'UTR reporter was monitored by RT-qPCR. The relative fold change in recovered RNA upon *Mkrn1* knockdown is illustrated, compared to RIP experiments in *LacZ*-depleted cells. For every RIP experiment, the enrichment was calculated using GFP. Error bars depict SEM, $n \geq 4$. (B) Bru1 binding to *luciferase-osk*-3'UTR upon *pAbp* knockdown was analyzed using GFP-RIP with subsequent RT-qPCR. The relative fold change in binding of GFP-Bru1 to *luciferase-osk*-3'UTR compared to control knockdown is illustrated. The individual enrichments were normalized to IP experiments using GFP alone. Error bars depict SEM, $n = 3$. (C) RIP experiments in either heterozygous (wild-type) or homozygous *Mkrn1^W* ovaries using α -Bru1 antibody. The relative fold change in recovered endogenous *osk* mRNA in wild-type compared to *Mkrn1^W* ovaries is depicted. As control RIP, normal IgG was used for every condition. Error bars indicate SEM, $n = 4$. (D-G) Immunostaining experiments showing Bru1 distribution in (D-E) wild-type and (F-G) *Mkrn1^W* early-stage egg chambers. Note the more prominent accumulation of Bru1 in the oocyte in the *Mkrn1* mutant. Scale bars, (D and F) 25 μ m; (E and G) 20 μ m. (H-M) Stage 10 egg chambers of the indicated genotypes immunostained with α -Osk. Posterior accumulation of Osk is restored to a variable degree (K-M) in *Mkrn1^W* oocytes when heterozygous for *bru1*. Scale bars, 25 μ m. (N) Quantification of posterior Osk localization in oocytes depicted in (H-M). The thresholds for weak, moderate, and strong are arbitrary. The photographs in the H-M panels illustrate what is meant by the different categories. $n = 21$ for wild-type, $n = 52$ for *Mkrn1^W*, $n = 100$ for *bru1/+; Mkrn1^W*. (O) Immunoblot analysis of protein lysates from ovaries depicted in (D-G). Heterozygous mutation of *bru1* led to an increase of Osk protein levels in *Mkrn1^W* ovaries.

<https://doi.org/10.1371/journal.pgen.1008581.g007>

survival rate of embryos produced from *Mkrn1^W* females that were heterozygous for *bru1^{QB}*, as compared to controls (620/2058, 30.1% vs 40/1222, 3.3%). Taken together, these experiments demonstrate that Mkrn1 activates *osk* translation, most likely by displacing Bru1 binding at the *osk* 3' UTR (Fig 8).

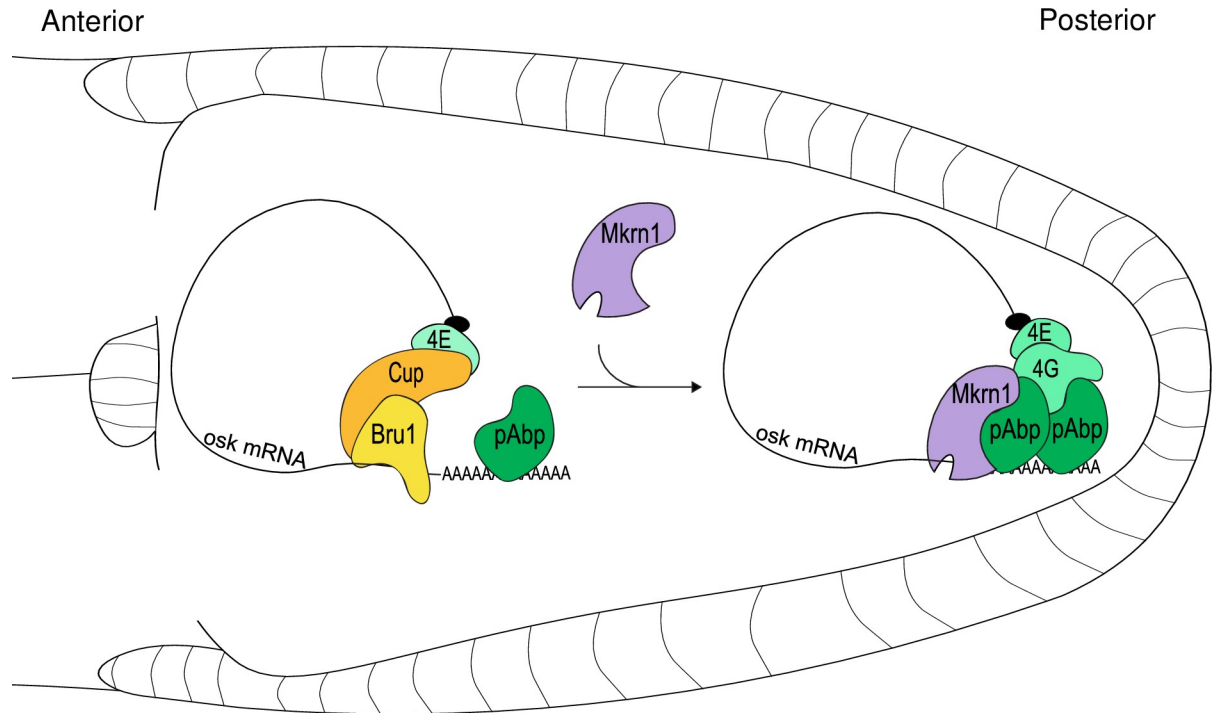


Fig 8. Model depicting activation of *osk* translation via *Mkrn1*. *Mkrn1* is recruited to the *osk* 3' UTR and stabilized by pAbp. The recruitment of *Mkrn1* leads to the displacement of Bru1 promoting translational activation at the posterior pole of the oocyte.

<https://doi.org/10.1371/journal.pgen.1008581.g008>

Discussion

Our data indicates that *Mkrn1* is essential for oogenesis, embryonic patterning, and germ cell specification. An essential role for *Mkrn1* in oogenesis has also been recently reported [53]. By taking advantage of a new allele that specifically disrupts *Mkrn1* binding to RNA, we demonstrate that *Mkrn1* exerts its function in embryogenesis and germ cell specification, primarily via regulating *osk* translation by antagonizing Bru1 binding.

Control of *osk* translation has been studied in depth, revealing a complex spatio-temporal interplay between repressing and activating factors [19]. Relief of translational repression and activation of *osk* translation is likely to involve multiple redundant mechanisms. For example, Bru1 can be phosphorylated on several residues, and phosphomimetic mutations in these residues inhibit Cup binding in pulldown assays. However, these do not seem to affect translational repression activity *in vivo* [24]. *Stau*, *Aub*, *Orb* and pAbp have also been implicated in activating *osk* translation [14,29,40,54]. However, it is unlikely that *Mkrn1* controls *osk* translation by recruiting *Stau*, as *Stau* still colocalizes with *osk* mRNA in *Mkrn1*^W oocytes (S12G–S12I Fig). Instead, we propose that *Mkrn1* exerts its positive activity by competing with Bru1 binding to *osk* 3' UTR (Fig 8). This is evidenced by the overlap of their binding sites, the increased association of Bru1 to *osk* mRNA upon *Mkrn1* knockdown and by our observation that reducing *bru1* dosage is sufficient to partially alleviate *osk* translational repression.

Two distinct Bru1 binding regions (AB and C) are present in the *osk* 3' UTR and are required for translational repression. However, the C region has an additional function in translational activation. Indeed, it was hypothesized that an activator binds the C region to relieve translational repression [25]. This activator was proposed to either be Bru1 itself, or a different protein that can bind the BRE-C, which is what we observed for *Mkrn1* (Fig 6A). Our results suggest that the interaction of pAbp with the nearby AR region, and the consequent

stabilization of Mkrn1 binding, contributes to the role of BRE-C in *osk* translational activation. Other factors may also be involved. For instance, Bicoid Stability Factor (BSF) binds the C region *in vitro* at the 3' type II Bru1-binding site [55], at a similar site to where Mkrn1 binds *osk*. Deletion of this site impacts embryonic patterning, yet depletion of BSF has no effect on Osk protein expression up to stage 10, indicating that initial activation of *osk* translation is effective even in the absence of BSF [55]. In this case, only late stage oocytes display reduced Osk accumulation. Therefore, it is possible that a concerted action of Mkrn1 and BSF exists at the *osk* 3' UTR site to activate translation and sustain it at later stages.

The binding of Mkrn1 to mRNA seems to be extremely specific. We found that the binding to *osk* is dependent on a downstream A-rich sequence and on interaction with pAbp. A few other targets we identified also display enrichment for downstream AA nucleotides (S13 Fig). and human MKRN1 has recently been shown to associate preferentially to such sequences [49]. Relevant to this, Bru1 binds to *grk* 3' UTR in addition to *osk* [56,57], and several proteins that associate with Mkrn1 also associate with *grk* mRNA [46,47]. However, we found no evidence that Mkrn1 binds specifically to *grk*, which lacks poly(A) stretches in the proximity of its Bru1 binding sites, and consistently, we did not observe a regulatory role of Mkrn1 on Grk translation.

In addition to pAbp, it is noteworthy that Mkrn1 associates with other proteins previously implicated in *osk* localization and translational activation. Its interaction with eIF4G would be consistent with a role in alleviating Cup-mediated repression, as it could recruit eIF4G to the cap-binding complex at the expense of Cup. However, we did not observe an interaction between Mkrn1 and eIF4E (S7C and S7D Fig, S1 and S2 Tables). The association between Mkrn1 and Imp is also intriguing as the *osk* 3' UTR contains 13 copies of a five-nucleotide motif that interacts with Imp [28]. This region is essential for *osk* translation but Osk accumulation is unaffected in *Imp* mutants, suggesting the involvement of another factor that binds these motifs [26,28,46]. In contrast to pAbp, we did not observe alteration of Mkrn1 binding when Imp was depleted, indicating that Imp is not required to stabilize Mkrn1 on *osk* mRNA.

The molecular links we uncovered between Mkrn1 and RNA-dependent processes in *Drosophila* are consistent with recent high-throughput analysis of mammalian MKRN1 interacting proteins [37,49]. RNA binding proteins, including PABPC1, PABPC4, and eIF4G1, were highly enriched among the interactors. Moreover, human MKRN1 was also recently shown to bind to RNA, dependent on the PAM2 motif and the interaction with PABPC1 [49]. In addition, the short isoform of rat MKRN1 was shown to activate translation but the underlying mechanism remained unknown [39]. Since in vertebrates MKRN genes are highly expressed in gonads and early embryos as well, it is possible that similar molecular mechanisms are employed to regulate gene expression at these stages [33]. Consistent with this, MKRN2 was recently found to be essential for male fertility in mice [58]. Thus, our study provides a mechanism that explains the role of Mkrn1 in translation and constitutes a solid framework for future investigations deciphering the roles of vertebrate MKRNs in post-transcriptional control of gene expression during gametogenesis and early development.

Materials and Methods

Generation of *Mkrn1* mutants using CRISPR/Cas9

The guide RNAs used were cloned into expression vector pDFD3-dU63gRNA (Addgene) according to manufacturer's instructions. Different guide RNAs were used either alone (gRNA1 starting at nucleotide 64 of *Mkrn1* CDS and gRNA2 starting at nucleotide 363 of *Mkrn1* CDS) or in combination (gRNA3 starting at 387 nt of *Mkrn1* gene and gRNA4 starting at position 2239 nt). *vas*-Cas9 *Drosophila* embryos were injected with the purified plasmids

containing the gRNA (500 ng/ μ l in H₂O) and allowed to develop to adulthood. Each male was crossed with double balancer females. Genomic PCR from single flies was prepared and tested for CRISPR/Cas9 induced mutations using the T7 endo I (BioLabs) assay or by PCR using primers that bind in proximity to the guide RNA targeting site. A list of gRNAs as well as primers is appended (S3 Table).

Immunostaining and confocal imaging

Ovaries were dissected and fixed in 4% paraformaldehyde in PBS for 20 min at room temperature (RT). After 4–5 washes in PBST (PBS containing 0.3% Triton-X100) ovaries were permeabilized with 1% freshly prepared Triton-X100 in PBS for 1 h. The ovaries were blocked in 2% BSA/PBST overnight. Dispersed egg chambers were then incubated with the primary antibodies diluted in 2% BSA/PBST at RT for 4 h or overnight at 4°C. The washed egg chambers were incubated with conjugated secondary antibodies at 1:500 at RT for 4 h or overnight at 4°C. DAPI (1 ng/ml) was added in the last wash to counter-stain the nuclei for 30 min. After 2–3 washes with PBST the mounting medium containing 1% DABCO was added and the samples were equilibrated for 30 min or overnight. The stained samples were mounted on glass slides and sealed with nail varnish for microscopy imaging. Rabbit polyclonal antibodies against Vas, Osk, Aub, Grk were generated in the Lasko lab; rabbit α -Stau is from the St Johnston lab; rabbit α -Bru1 is from the Ephrussi lab and rabbit α -pAbp is from the Sonenberg lab; mouse monoclonal antibodies against Orb, Sqd, and Lamin were purchased from the Developmental Studies Hybridoma Bank; mouse α -GFP and rabbit α -Flag were purchased from Abcam and Sigma. Alexa Fluor 488 or 555 conjugated secondary antibodies were purchased from Molecular Probes, and pre-absorbed with fixed and blocked wild type ovaries to reduce background. Stained egg chambers were examined using a confocal microscope (Leica). Images were taken under 40 x oil lens by laser scanning and processed with ImageJ.

In situ hybridization of embryos and ovaries and RNA-protein double labeling

cDNAs were used as templates for PCR to generate an amplified gene fragment with promoter sequences on each end. PCR products were purified via agarose gel extraction and used for *in vitro* transcription to generate digoxigenin-labeled RNA antisense probes with MAXIscript kit (Ambion). The length of each probe was about 1000 nt. *In situ* hybridization experiments were performed as described [59], using biotinylated α -DIG antibody and streptavidin-HRP followed by tyramide conjugation for development of FISH signal. For RNA-protein double labeling, ovaries or embryos were incubated in primary antibody against the protein of interest along with biotinylated α -DIG antibody at 4°C overnight. The tissue was washed, then detection reagent (fluorochrome-conjugated secondary antibody) along with streptavidin-HRP was added and incubated at 4°C overnight. Images were taken with confocal microscope (Leica).

Embryo cuticle preparation and staining

Flies were transferred into egg-laying cages with apple juice agar plates and incubated at 25°C in the dark. Embryos were collected when 50–100 eggs had been laid and allowed to age for 24 h at 25°C. Embryos were collected in a sieve, dechorionated with 50% bleach for 2.5 min, washed with water, then transferred into PBST buffer (PBS + 0.1% Tween 20). For cuticle preparations, PBST buffer was removed, then 40–50 μ l of Hoyer's solution was added and embryos were kept at 4°C overnight. Embryos in Hoyer's solution were mounted on a glass slide, covered with a cover slip and incubated at 60–65°C overnight. Dark-field images were taken with Leica DM6000B microscope.

Staging

Staging experiment was performed as described [60] using *D. melanogaster* *w*¹¹¹⁸ flies.

Generation of transgenic flies

The constructs were made using Gateway technology (Invitrogen). Full-length wild-type *Mkrn1* cDNA was cloned into the pENTR entry vector using the pENTR/D-TOPO cloning kit (ThermoFisher). After verifying the sequence by PCR, the insert was subcloned into the expression vectors containing UASp promoter with different tags (pPVW and pPFW with Venus and FLAG tags at N-terminal respectively), and (pPWV and pPWF with Venus and FLAG tags at C-terminal respectively) by LR in vitro recombination. For *Mkrn1*^{ΔZnF1} pPFMW vector was used. Constructs were verified by sequencing and then injected into *yw* embryos. Progeny harboring the transgenes were crossed with double balancer flies to establish a variety of lines, and the insertion sites were mapped to either the second or third chromosome. *Mkrn1* expression was then driven by crossing the transgenic lines with a *nos>Gal4* line (MTD). Expression of tagged *Mkrn1* was verified by western blot analysis and immunostaining using anti-GFP (Abcam) or anti-FLAG (Sigma).

Rescue experiment

Flies carrying Venus- or FLAG-*Mkrn1* on the second chromosome were crossed with the *nos>Gal4* driver lines in three different *Mkrn1* mutant backgrounds (*Mkrn1*^W, *Mkrn1*^S, and *Mkrn1*^N). Progeny were collected and separated into two groups: (1) *Venus- or FLAG-Mkrn1/nos>Gal4; Mkrn1*^{W(S or N)/Mkrn1}^{W(S or N)} and (2) *nos>Gal4/CyO; Mkrn1*^{W(S or N)/Mkrn1}^{W(S or N)}. To perform hatching tests the same number of flies from each group was fed with yeast butter on apple juice plates for 1 d, embryos were collected and incubated at 25°C for 48 h to allow completion of hatching. Hatched and unhatched embryos were counted for each group. The data from several tests in the same group were pooled and the hatching percentage was calculated.

Cell line

Drosophila S2R+ are embryonic derived cells obtained from Drosophila Genomics Resource Center (DGRC, Flybase ID: FBtc0000150).

Cell culture, RNAi, transfection

Drosophila S2R+ cells were grown in Schneider's medium (Gibco) supplemented with 10% FBS (Sigma) and 1% Penicillin-Streptomycin (Sigma). For RNAi experiments, PCR templates for the dsRNA were prepared using T7 Megascript Kit (NEB). S2R+ cells were seeded at the density of 10⁶ cells/ml in serum-free medium and 15 μg/ml of dsRNA was added to the cells. After 6 h of cell starvation, serum supplemented medium was added to the cells. dsRNA treatment was repeated after 48 h and cells were collected 24 h after the last treatment. A list of primers used to create dsRNA templates by PCR is appended (S4 Table). Effectene (Qiagen) was used to transfect vector constructs in all overexpression experiments following the manufacturer's protocol.

Immunoprecipitations (IPs)

For IP experiments in S2R+ cultured cells, protocol was followed as described [60] with minor changes: 2 mg of the protein lysates was incubated for 2 h with 10 μl of either Myc-Trap or GFP-Trap beads (Chromotek). To determine the dependence of interactions on RNA, 50 U of

RNaseT1 (ThermoFisher) were added to the respective IP. To ensure the activity of RNase T1, lysates were incubated 10 min at RT prior to the incubation of lysate with antibody.

For IP experiments in ovaries, 150 μ l of wet ovaries from 3–5 day old flies expressing Venus-Mkrn1 was homogenized on ice in 2 ml of cold IP buffer (1 X PBS, 0.4% Triton X-100, 1 mM MgCl₂, 5% glycerol), containing protease inhibitors and PMSF. The extracts were diluted to 1.5 mg protein/ml. Each extract (0.66 ml) was mixed with 24 μ g of anti-pAbp Ab antibody (Smibert lab, [61]), 17 μ g of α -eIF4G rabbit antibody, or 15 μ l of rabbit anti- α -Tubulin antibody (Abcam). When present, 100 μ g RNase A (Qiagen) was added to the samples. Samples were incubated with rotation at 4°C overnight, then mixed with 30 μ l of protein A agarose beads (wet volume, Invitrogen) and incubated with rotation at RT for 1.5 h. The beads were washed three times with IP buffer. Bound material on the beads was eluted by boiling for 2 min in 40 μ l of SDS loading buffer. 20 μ l of the eluted sample, together with input samples, was used for western blot.

RNA- Immunoprecipitation (RIP)

For RIP, S2R+ cells or ovaries were harvested and lysed in RIP buffer (150 mM NaCl, 50 mM Tris-HCl pH 7.5, 0.5% NP-40, 1 mM EDTA) supplemented with proteinase inhibitors (1.5 μ g/ml Leupeptin, 1.5 μ g/ml Pepstatin, 1.5 μ g/ml Aprotinin and 1.5 mM PMSF) and RNase inhibitors (20 U/ μ l). S2R+ cells were lysed for 20 min at 4°C, subjected to 2 cycles of sonication on a bioruptor (Diagenode) with 30 sec “ON”/“OFF” at low setting and the remaining cell debris was removed by centrifugation at 21,000 g for 10 min at 4°C. To remove lipids and cell debris, ovary lysates were centrifuged 4 times. Protein concentrations were determined using Bradford reagent (BioRad). 2 mg of protein lysate were incubated for 3 h with 2 μ g of α -FLAG M2 antibody (Sigma-Aldrich) pre-coupled to 20 μ l of protein G Dynabeads (Thermo Fisher Scientific) head-over-tail at 4°C. For RIP experiments analysing binding of Bru1 in ovaries, either 1 μ l of rabbit α -Bru1 (gift from A. Ephrussi) or 2 μ g of rabbit IgG (Millipore) were incubated with ovarian lysate over night at 4°C. 20 μ l of protein G Dynabeads were added for 2 h after the incubation. For every RIP experiment, beads were washed 4 x for 10 min in RIP buffer at 4°C.

For immunoprecipitation of GFP-tagged Imp and Bru1 15 μ l of GFP-Trap (Chromotek) were used. Lysates were prepared similar as above using RIPA buffer (140 mM NaCl, 50 mM Tris pH 7.5, 1 mM EDTA pH 8, 1% Triton X-100, 0.1% SDS, 0.1% sodium deoxycholate) supplemented with proteinase and RNase inhibitors. IP was performed for 2 h at 4°C and subsequently washed 4 x for 10 min with RIPA buffer.

RNA was eluted in TRIzol Reagent (ThermoFisher), 10 min at RT and subjected to RNA isolation and RT-qPCR. To obtain the depicted fold enrichment, individual transcripts were normalized to either *18S* or *RpL15* (S5 Table). At least three biological replicates were performed for each experiment. If not stated differently statistical analysis was performed using one sample t-test.

To analyze IPs, 30% of beads were eluted in 1x SDS buffer (50 mM Tris pH 6.8, 2% SDS, 10% glycerol, 100 mM DTT, 0.05% Bromphenol Blue) at 95°C for 10 min. Eluted IP proteins were removed from the beads and analyzed by western blot together with input samples.

Western blotting

Western blotting was performed as described [60]. Primary antibodies used were: mouse α -Myc 9E10 antibody (1:2000, Enzo Life Sciences); mouse α -FLAG M2 antibody (1:1000, Sigma-Aldrich); rabbit α -GFP TP401 antibody (1:5000, Acris Antibodies); mouse α -HA F7 (1:1000, Santa-Cruz) rat α -HA (1:750, Roche); mouse α - β -Tubulin (1:5000, Covance), mouse α - α -

Tubulin (1:20,000; Sigma), mouse α -GFP (1:500; Molecular probe), mouse α -ubiquitin (1:1000; Santa Cruz) Fab α -pAbp (2.5 μ g in 5 ml), α -eIF4G rabbit antibody (1 μ g in 5 ml), rabbit α -Osk (1:1000) antibody was a gift from A. Ephrussi.

RNA isolation and measurement of RNA levels

Cells or tissues were harvested in TRIzol Reagent (ThermoFisher) and RNA was isolated according to the manufacturer's instructions. DNA was removed with DNaseI treatment (NEB) and cDNA was prepared with M-MLV Reverse Transcriptase (Promega). The transcript levels were quantified using Power SYBR Green PCR Master Mix (ThermoFisher) using the indicated primer ([S5 Table](#)).

LC-MS/MS

To identify binding partners of Mkrn1, either Myc-GFP as control or Myc-Mkrn1 were ectopically expressed in S2R+ cells. Upon lysis, Myc-GFP or Myc-Mkrn1 were immunoprecipitated as described above (see IP methods) with small adjustments: The IP buffer was additionally supplemented with 10 mM N-ethylmaleimide, 1 mM sodium orthovanadate, 5 mM β -glycerophosphate and 5 mM sodium fluoride. After IP, samples were eluted in 2x LDS buffer (Life Technologies) supplemented with 1 mM dithiothreitol for 10 min at 70°C and incubated with 5.5 mM 2-chloroacetamide for 30 min at room temperature in the dark. All samples were prepared in parallel.

Conventional interactome analysis of the IP samples was performed as described before [62] with the following changes: The enriched proteins were separated by SDS-PAGE with a 4–12% Bis-Tris protein gel (NuPAGE, Thermo Scientific) and stained with Colloidal Blue Staining Kit (Life Technologies). Subsequently, proteins were in-gel digested using trypsin and digested peptides were then extracted from the gel. Concentration, clearance and acidification of peptides, mass spectrometry analysis, and peptide identification were performed as described before [62]. For peptide identification in MaxQuant (version 1.5.28), the DROME database from UniProtKB (release May 2016) was used. For label-free quantification (LFQ) at least 2 LFQ ratio counts (without fast LFQ) were activated.

The data table of LFQ values resulting from MaxQuant was filtered for potential contaminants, reverse binders and protein groups only identified by site. Furthermore, protein groups with less than two peptides and less than one unique peptide were also removed from further analysis. After log-transforming all remaining LFQ values, missing values were imputed by beta distributed random numbers between 0.1% and 1.5% of the lowest measured values. As a final filtering step, only protein groups having measured values for at least two replicates of at least one experimental condition were kept for further analysis. All filter and imputing steps were done with an in-house R script.

Differential protein abundance analysis was performed on log-transformed LFQ values between two conditions at the time using the R package limma (version 3.34.9, [63]). For each such comparison, only protein groups found in at least two replicates of at least one condition were kept and used. To visualize the interactome, the R package ggplot2 [64] was used. All protein groups with an $FDR \leq 0.05$ and a \log_2 fold change of ≥ 2 were considered significantly changed.

The mass spectrometry proteomics data have been deposited to the ProteomeXchange Consortium via the PRIDE partner repository with the dataset identifier PXD011802.

PAM2 motif alignment

Ortholog searches were performed using HaMStR-OneSeq [65]. Human MKRN1 and MKRN2 (UniProt identifiers: Q9UHC7, Q9H000) served as seed proteins and orthologs were searched within data from the Quest for Orthologs Consortium (release 2017_04, [66]). In order to identify functionally equivalent proteins, we calculated a unidirectional Feature Architecture Similarity (FAS) score that compares the domain architecture of the seed protein and the predicted ortholog [67]. Predicted orthologs with FAS < 0.7 were removed. The multiple sequence alignment of PAM2 motifs of Makorin orthologs from selected arthropod and vertebrate species was generated using MAFFT v7.294b L-INS-i [68]. Since the PAM2 motif in all Makorin proteins differs from the described consensus, a PAM2 hidden Markov model was trained on Makorin PAM2 motifs and used for a HMMER scan (<http://hmmer.org/>) of the orthologs. Orthologs include species name, UniProt identifiers and amino acid (aa) positions of the PAM2 motif within the protein: *Drosophila melanogaster*, Q9VP20, 81–95 aa; *Anopheles gambiae*, Q7QF83, 57–71 aa; *Tribolium castaneum*, A0A139WP96, 159–173 aa; *Ixodes scapularis*, B7QIJ9, 119–133 aa; human, Q9UHC7, 163–177 aa; mouse, Q9QXP6, 163–177 aa; zebrafish, Q4VBT5, 120–134 aa.

Individual-nucleotide resolution UV CrossLinking and ImmunoPrecipitation (iCLIP) and autoradiography

The iCLIP protocol was performed as in [69] with the following adaptations: S2R+ cells were crosslinked with 150 mJ/cm² of UV light and subsequently harvested. Cells were lysed in urea cracking buffer (50 mM Tris pH 7.5, 6 M urea, 1% SDS, 25% PBS) and sonicated using 2 cycles with 30 sec “ON”/“OFF” at low setting. Remaining cell debris was removed by centrifugation at 21,000 x g for 10 min at 4°C. Lysate was diluted 1:5 in IP buffer (150 mM NaCl, 50 mM Tris pH 7.5, 0.5% Tween-20, 0.1 mM EDTA) and incubated with 4 µg of anti-FLAG M2 antibody (Sigma-Aldrich) pre-coupled to 100 µl of protein G Dynabeads (ThermoFisher Scientific) for 2 h at 4°C. After IP, the pulled-down RNA-protein complexes were washed 3x with high salt buffer (1 M NaCl, 50 mM Tris pH 7.4, 1 mM EDTA, 1% NP-40, 0.1% SDS, 0.5% Na-DCC) and 3x with PNK buffer (10 mM MgCl₂, 20 mM Tris pH 7.6, 0.2% Tween-20). To trim the length of the crosslinked RNA, on-bead digestion using Turbo DNase (Ambion) and RNase I (Ambion) was performed. Subsequently, the beads were washed again 3x with high salt buffer and 3x with PNK buffer.

For high-throughput sequencing of iCLIP experiments, libraries of 6 technical replicates for FLAG-Mkrn1 and 1 replicate for FLAG-GFP (Control) were prepared as described [69]. Barcodes used for the libraries are listed in S6 Table. Multiplexed iCLIP libraries were sequenced as 75-nt single-end reads on an Illumina MiSeq sequencing system.

Sequencing qualities were checked for all reads using FastQC (version 0.11.5) (<https://www.bioinformatics.babraham.ac.uk/projects/fastqc/>). Afterwards, reads were filtered based on sequencing qualities (Phred score) of the barcode region. Reads with more than one position with a Phred score < 20 in the experimental barcode (positions 4 to 7 of the reads) or any position with a Phred score < 17 in the random barcode (positions 1 to 3 and 8 to 9) were excluded from subsequent analysis. Remaining reads were de-multiplexed based on the experimental barcode (positions 4 to 7) using Flexbar (version 3.0.0, [70]) without allowing any mismatch.

All following steps of the analysis were performed on the individual samples after de-multiplexing. Remaining adapter sequences were removed from the read ends using Flexbar (version 3.0.0) with a maximal error rate of 0.1 and a minimal overlap of 1 nt between the beginning of the adapter and the end of the read. Following adapter trimming, the first 9 nt of each read containing the experimental and random barcodes were trimmed off and added to the read name in the fastq files in order to keep this information for downstream analysis. Reads shorter than 15 nt were removed from further analysis.

Trimmed and filtered reads were mapped to the *Drosophila melanogaster* genome (Ensembl genome assembly version BDGP6) and its annotation (Ensembl release 90, [71]) using STAR (version 2.5.2b, [72]). When running STAR, up to two mismatches were allowed, soft-clipping was prohibited at the 5' ends of reads and only uniquely mapping reads were kept for further analysis. For further analysis, only unspliced reads were kept and analyzed.

Following mapping, duplicate reads were marked using the dedup function of bamUtil (version 1.0.13), which defines duplicates as reads whose 5' ends map to the same position in the genome (<https://github.com/statgen/bamUtil>). Subsequently, marked duplicates with identical random barcodes were removed since they are considered technical duplicates, while biological duplicates showing unequal random barcodes were kept.

Resulting bam files were sorted and indexed using SAMtools (version 1.3.1, [73]). Afterwards, bedgraph files were created based on bam files, using bamToBed of the BEDTools suite (version 2.25.0; [74]), considering only the position upstream of the 5' mapping position of the read, since this nucleotide is considered as the crosslinked nucleotide. Using bedGraphToBigWig of the UCSC tool suite [74], all bedgraph files were converted into BigWig files [75].

In order to estimate binding site strength and to facilitate comparisons between binding sites (S10D Fig) we corrected for transcript abundance by representing the crosslink events within a binding site as a 'signal-over-background' ratio (SOB). The respective background was calculated as the sum of crosslink events outside of binding sites (plus 5 nt to either side) by the merged length of all exons. 3' UTR lengths were restricted to 10 nt past the last Mkrn1 binding site or 500 nt if no binding site was present. SOB calculations were performed separately for each replicate and then averaged. No SOB value was assigned for ribosomal genes and genes with a background of < 10 crosslink events, resulting in SOB values for 184 binding sites in 46 targets.

The sequence content around the predicted Makorin 1 binding sites was estimated by counting homopolymeric 2-mers (S13 Fig). All 262 binding sites that fall in 3' UTRs were centered at their midpoint and a symmetric window was extended 100 nucleotides up- and downstream. For each position the mean occurrence of each 2-mer was counted.

The iCLIP data has been deposited to the NCBI's Gene Expression Omnibus [76] and is accessible through GEO Series accession number GSE123052 (<https://www.ncbi.nlm.nih.gov/geo/query/acc.cgi?acc=GSE123052>).

Cloning

To overexpress tagged proteins, the respective coding sequences were amplified and cloned into Gateway plasmids using *AscI* and *NotI* restriction sites for plasmids pPFMW and pAHW. The coding sequences of *Imp*, *bru1* and *pAbp* were cloned using *KpnI* and *XbaI* into plasmid pAWG. A list of primers used to introduce the coding sequences as well as to introduce mutations in the *Mkrn1* coding sequence is appended (S7 Table). To analyze the binding of Mkrn1 to *osk*, either the 3' UTR was cloned downstream of Firefly coding sequence or the complete *osk* gene was cloned in the same vector backbone of pAc5.1B-EGFP (gift from Elisa Izaurralde, Addgene plasmid #21181). For both, restriction sites of *KpnI* and *SalI* were used. To ensure the proper usage of the endogenous poly(A) signal the *osk* 3' UTR and the *osk* gene included 220 and 248 nucleotides of the downstream sequence, respectively. The primers used for cloning and to introduce mutations are listed in S8 Table.

Supporting information

S1 Fig. Four Makorin-related genes are expressed in *Drosophila melanogaster*. (A) Sequence alignment of human MKRN1 and the four Makorin-related proteins in *Drosophila*, Mkrn1, CG5334, CG5347, and CG12477. The ZnF1 domain in Mkrn1 is highlighted green, the PAM2

motif is highlighted yellow, the RING domain is highlighted red, and the ZnF2 domain is highlighted light blue. The RING and ZnF2 domains are conserved in all four proteins, whereas the PAM2 motif is only conserved in CG12477 and CG5347, and ZnF1 is conserved in CG5334 and CG5347. (B) Relative mRNA levels of *Mkrn1* and the three other genes encoding predicted Makorin proteins at various stages of development, as measured by RT-qPCR. mRNA levels were normalized to *Rpl15* mRNA. Error bars depict Stdev, $n = 3$.

(TIF)

S2 Fig. Mkrn1 colocalizes with pole plasm components. All images are from wild-type oocytes expressing Venus-Mkrn1 or FLAG-Mkrn1 as indicated. Overexpression was performed using a *nos>Gal4* driver. (A, D,) Immunostaining with α -FLAG to monitor FLAG-Mkrn1. (G and J) Immunostaining with α -GFP recognizing Venus-Mkrn1. (B and E) Immunostaining with α -Osk. (H and K). (C, F, I, L,) Merged images from two preceding panels. Scale bars: (A-C, G-I,) 5 μ m; (D-F, J-L) 20 μ m.

(TIF)

S3 Fig. Effects of *osk* and *vas* mutations on Mkrn1 localization. (A) Posterior accumulation of either Venus-Mkrn1 or FLAG-Mkrn1 is normal in *osk*^{54/+} oocytes but is absent in *osk*^{54/Df(3R)p-XT103 (*osk*) oocytes. (B) Posterior accumulation of either Venus-Mkrn1 or FLAG-Mkrn1 is normal in both *vas*^{1/+} or *vas*^{1/vas}^{PH} (*vas*) oocytes. Scale bars, 50 μ m.}

(TIF)

S4 Fig. Mkrn1 genetically interacts with *osk* and *vas*. Pole cell counts from embryos produced by females with the indicated genotypes. Embryos from trans-heterozygotes for *Mkrn1* and *osk* or *vas* mutations have fewer pole cells than those from single heterozygote controls. Error bars illustrate Stdev, $n = 60$.

(TIF)

S5 Fig. Transgenic expression of tagged Mkrn1 rescues all Mkrn1 mutant phenotypes.

(A-C) Bright-field micrographs of entire ovaries from (A) *Mkrn1*^N; (B) *nos>FLAG-Mkrn1; Mkrn1*^N and (C) wild-type females, showing overall rescue of oogenesis. Scale bars, 500 μ m. (D-F) α -Osk immunostaining on (D) *Mkrn1*^W, (E) *Mkrn1*^S, (F) *Mkrn1*^N egg chambers as negative controls. (G-J) Transgenic expression of tagged *Mkrn1* restores posterior localization of Osk protein in *Mkrn1*^W oocytes. (G, H) *nos>Venus-Mkrn1; Mkrn1*^W; (I and J) *nos>FLAG-Mkrn1; Mkrn1*^W. (H and J) Immunostaining with α -Osk; (G) Immunostaining with α -GFP to visualize Venus-Mkrn1; (I) Immunostaining with α -FLAG recognizing FLAG-Mkrn1. (K-N) Transgenic expression of tagged *Mkrn1* restores expression and posterior localization of Osk protein in *Mkrn1*^S oocytes. (K and L) *nos>Venus-Mkrn1; Mkrn1*^S; (M and N) *nos>FLAG-Mkrn1; Mkrn1*^S. (L and N) Immunostaining using α -Osk; (K) Immunostaining with α -GFP recognizing Venus-Mkrn1; (M) Immunostaining using α -FLAG to visualize FLAG-Mkrn1. (O and P) Transgenic expression of tagged *Mkrn1* restores expression and posterior localization of Osk protein in *Mkrn1*^N oocytes. (Q-T) Immunostaining experiments revealing localization of various proteins in *nos>Venus-Mkrn1; Mkrn1*^N oocytes. (Q) α -Stau; (R) α -Vas; (S) α -Aub; (T) α -Grk. (D-T) Scale bars, 50 μ m.

(TIF)

S6 Fig. Mkrn1 mutations affect accumulation of mRNAs involved in axis patterning in embryos. (A and B) Antero-dorsal accumulation of *grk* mRNA is similar to wild-type in stage 10 *Mkrn1*^W oocytes. Scale bars, 50 μ m. (C) *grk* mRNA remains associated with the oocyte nucleus and is mislocalized to the posterior in stage 10 *Mkrn1*^S oocytes. Scale bars, 50 μ m. *In situ* hybridization experiments showing posterior accumulation of (D) *osk*, (E) *nos*, and (F) *pgc*

mRNAs in wild-type embryos. Scale bars, 100 μm . (G-I) Posterior accumulation of these mRNAs is lost in *Mkrn1^W* embryos. Scale bars, 100 μm .

(TIF)

S7 Fig. Interactome of Mkrn1 in S2R+ cells. (A) Schematic diagram of Mkrn1 constructs with functional domains highlighted. Different mutations were introduced into Mkrn1 protein: Mkrn1^{RING} carries a point mutation that changes histidine 239 to glutamic acid (H239E) while Mkrn1 ^{Δ ZnF1} contains a deletion of amino acids 26 to 33. To disrupt the ZnF2 domain (Mkrn1^{ZnF2}) three point mutations that mutate cysteines to alanines at positions 302, 312 and 318 (C302A, C312A and C318A) were introduced. (B) Immunoblot showing the relative expression levels of various forms of FLAG-Mkrn1 in S2R+ cells. (C, D) Volcano plots showing the interactome of (C) Myc-Mkrn1 and (D) Myc-Mkrn1^{RING} in S2R+ cells identified using LC-MS/MS and label-free quantification. For both experiments, 3 technical replicates of Myc-GFP (ctrl) and Myc-Mkrn1 IP were performed and compared with each other. The enrichment of proteins compared to the control was plotted in a volcano plot using a combined cut-off of \log_2 fold change ≥ 2 and an FDR ≤ 0.05 . Several proteins of interest are labelled. The entire list of enriched proteins can be found in S1 and S2 Tables.

(TIF)

S8 Fig. Validation of Mkrn1 interactome. Pulldown experiments to validate binding of tagged Mkrn1^{RING} with (A) GFP-pAbp, (B) GFP-Imp, (C) Myc-eIF4G (D) Myc-Sqd and (E) Myc-Me31B. GFP and Myc IPs were performed in the absence or presence of RNase T1 and enrichment of the proteins was analyzed by immunoblotting. As controls, either GFP alone or Myc-GFP were used. All co-IP experiments were performed in S2R+ cells. (F) Western blot depicting co-IP experiments between Venus-Mkrn1 and eIF4G in ovaries. α -tubulin (α tub, lanes 1, 2) and ovaries lacking the *Venus-Mkrn1* transgene (lane 4) were used as negative controls.

(TIF)

S9 Fig. Analysis of the PAM2 motif. Rescue experiments of either Mkrn1 or Mkrn1^{PAM2} in *Mkrn1^N* ovaries. FLAG-tagged *Mkrn1* transgenes were overexpressed in ovaries using a *nos>Gal4* driver line. Ovaries were stained with α -1B1 (red) and α -Osk (green). Nuclei were stained using DAPI (blue). Although overexpression of wild-type Mkrn1 could restore Osk protein at the posterior, Mkrn1^{PAM2} could not. Scale bar, 50 μm .

(TIF)

S10 Fig. Analysis of the RNA binding ability of Mkrn1. (A) The RNA binding activity of Mkrn1 is mediated by its ZnF1 domain. Autoradiographs showing association of various forms of Mkrn1 to RNA. FLAG-tagged GFP was used as a negative control. Crosslinked RNA-protein complexes were immunoprecipitated with α -FLAG and treated with different dilutions of RNase I (left: 1/50, right: 1/5000). RNA was subsequently radiolabelled and the RNA-protein complexes were separated by SDS-PAGE. Bound RNA of different sizes is detected by a smear extending upward from the sharp bands that correspond to the sizes of the FLAG-Mkrn1 proteins (arrow). (B) Representative immunoblot of RIP experiment shown in Fig 6A. Either Mkrn1 or Mkrn1 ^{Δ ZnF1} were overexpressed in *Mkrn1^N* ovaries using a *nos>Gal4* driver. The proteins were immunoprecipitated using α -FLAG antibody. Note that Mkrn1 ^{Δ ZnF1} protein runs higher because of the presence of an additional Myc tag. (C) Validation of iCLIP experiments. Immunoprecipitation of FLAG-Mkrn1 was performed in different conditions. S2R+ cells were transfected and UV-crosslinked prior to IP experiments. Left: autoradiograph showing protein-RNA complexes. Right: Signals of lanes 2, 4 and 5 in autoradiograph were cut and RNA was subsequently isolated. RNA length was analyzed on a TBE-urea gel. (D) iCLIP

datasets with Mkrn1-FLAG in S2R+ cells. The x axis displays maximum binding strength per gene (SOB) and the y axis shows the gene identity. The genes are sorted by SOB with *osk* mRNA appearing at the third place. Note that ribosomal genes have been excluded for clarity. (TIF)

S11 Fig. Mkrn1 binding to *osk* 3' UTR is dependent on pAbp. (A) Mkrn1, but not Mkrn1^{ΔZnF1} binds to the *osk* 3' UTR in S2R+ cells. FLAG-RIP of GFP, Mkrn1 and Mkrn1^{ΔZnF1} was performed co-expressing either *luciferase-grk-3'UTR* or *luciferase-osk-3'UTR* reporter. Top: qPCR analysis of the RIP experiments. Fold enrichment is illustrated relative to GFP RIP. Error bars depict SEM, n = 3. Bottom: Immunoblots of a representative RIP experiment. (B-F) Western blot analysis of a representative FLAG-RIP experiment in S2R+ cells summarized in Fig 6C–6F. (B) Either FLAG-tagged GFP or Mkrn1^{RING} was overexpressed. RIP experiments were performed in the presence of a *luciferase-osk-3'UTR* reporter containing *osk* 3' UTR wild-type sequence or deletion of the Mkrn1 binding site (*osk*^{ΔMkrn1}) (C) FLAG-RIP of GFP or Mkrn1^{RING} were performed either using the *luciferase-osk-3'UTR* reporter. Binding was compared between wild-type *osk* 3' UTR and a mutation in the AR region (*osk*^{ΔAR}). (D and E) RIP experiments against FLAG-Mkrn1^{RING} were performed in control (*LacZ*) condition and compared to (D) *Imp* or (E) *pAbp* mRNA knockdown. Right: RT-qPCR analysis of the knockdown efficiency. *Imp* and *pAbp* mRNA levels were normalized to *Rpl15* mRNA. (F) FLAG-RIP experiments in S2R+ cells using different Mkrn1 mutants. Representative immunoblot is depicted. (TIF)

S12 Fig. Binding of Bru1 to *osk* 3'UTR is antagonized by Mkrn1. (A) RIP experiments of GFP alone or GFP-Bru1 in S2R+ cells. Left: qPCR analysis of RIP experiments analyzing the enrichment of the *luciferase-osk-3'UTR* transcript. Error bars depict SEM n = 3. Right: Immunoblot of one representative IP using α-GFP. (B-F) Immunoblots of representative RIP experiments summarized in Fig 7A–7C. Right: RT-qPCR validation of the respective knockdown. mRNA levels were normalized to *Rpl15* mRNA. (B) RIP experiment of either GFP alone or GFP-Bru1 were performed in control (*LacZ*) or *Mkrn1* mRNA knockdown condition. (C) GFP-RIP experiments were performed in control (*LacZ*) or *Mkrn1* mRNA knockdown condition for either GFP or GFP-*Imp*. (D) RIP experiment performed against FLAG-tagged pAbp or Sqd in *LacZ* or *Mkrn1* mRNA depleted cells. As control, RIP was performed with FLAG-tagged GFP. (E) GFP-RIP of either GFP alone or GFP-Bru1 in control (*LacZ*) or *pAbp* KD. (F) Representative immunoblot of a RIP experiment using heterozygous (wild-type) or homozygous *Mkrn1*^W ovary lysate against endogenous Bru1. As control RIP, normal rabbit IgG was used. (G-I) The three panels show the same *Mkrn1*^W stage 10 egg chamber stained for (G) Stau, (H) *osk* mRNA and (I) a merged image. There is accumulation of Stau near the pole plasm and co-localization with *osk* mRNA. Scale bar, 20 μm. (TIF)

S13 Fig. Makorin1 binding sites display a slight enrichment of “A” nucleotides. Homopolymeric dimers were counted in 200 a nucleotide wide window centered at 262 binding sites midpoints in 3' UTRs. (TIF)

S1 Table. List of identified interaction partners of Myc-Mkrn1 compared to Myc-GFP using mass spectrometry and limma analysis. All proteins with an FDR ≤ 0.05 05 and log₂ fold change ≥ 2 are depicted. (see supplementary file 1) (XLSX)

S2 Table. List of identified interaction partners of Myc-Mkrn1RING compared to Myc-GFP using mass spectrometry and limma analysis. All proteins with an FDR ≤ 0.05 and \log_2 fold change ≥ 2 are depicted. (see supplementary file 1).

(XLSX)

S3 Table. List of gRNAs used in this study and primers used to validate mutations of the *Mkrn1* gene by CRISPR/ Cas9.

(DOCX)

S4 Table. List of primers used to create PCR templates of dsRNAs.

(DOCX)

S5 Table. List of primers used to in qPCR experiments.

(DOCX)

S6 Table. List of barcodes used to prepare iCLIP libraries from material of S2R+ cells.

(DOCX)

S7 Table. List of primers used to clone CDSs of proteins as well as primers that were used to introduce mutations in the respective CDS.

(DOCX)

S8 Table. List of primers used to clone *osk* and *grk* reporter genes and introduce the mutations analyzed.

(DOCX)

Acknowledgments

We would like to thank the Bloomington Drosophila Stock Center for fly reagents, and Anne Ephrussi, Craig Smibert, Daniel St Johnston, and Nahum Sonenberg for antibodies. We also thank Violeta Morin and Beili Hu for fly embryo injections, the IMB Proteomics Core Facility for help with the initial analysis of the mass spectrometry data and the IMB Core Facility Genomics for their helpful support and use of its Illumina MiSeq machine. We also would like to thank the IMB Core Facility Microscopy for support and use of the TCS SP5 inverted microscope P.L. is grateful for sabbatical leave support from the Excellence Initiative of Radboudumc.

Author Contributions

Conceptualization: Jean-Yves Roignant, Paul Lasko.

Formal analysis: Mirko Brüggemann, Cornelia Rücklé, Anke Busch.

Investigation: Annabelle Dold, Hong Han, Niankun Liu.

Methodology: Andrea Hildebrandt, Heike Hänel.

Supervision: Petra Beli, Kathi Zarnack, Julian König, Jean-Yves Roignant, Paul Lasko.

Writing – original draft: Annabelle Dold, Hong Han, Niankun Liu.

Writing – review & editing: Jean-Yves Roignant, Paul Lasko.

References

1. Lasko P. 2012. mRNA localization and translational control in *Drosophila* oogenesis. *Cold Spring Harb Perspec Biol* 4(10): a012294.

2. Jambor H, Surendranath V, Kalinka AT, Mejstrik P, Saalfeld S, Tomancak P. 2015. Systematic imaging reveals features and changing localization of mRNAs in *Drosophila* development. *eLife* 4: e05003.
3. Lécuyer E, Yoshida H, Parthasarathy N, Alm C, Babak T, Cerovina T, et al. 2007. Global analysis of mRNA localization reveals a prominent role in organizing cellular architecture and function. *Cell* 131: 174–187. <https://doi.org/10.1016/j.cell.2007.08.003> PMID: 17923096
4. Zimyanin VL, Belaya K, Pecreaux J, Gilchrist MJ, Clark A, Davis I, et al. 2008. In vivo imaging of *oskar* mRNA transport reveals the mechanism of posterior localization. *Cell* 134: 843–853. <https://doi.org/10.1016/j.cell.2008.06.053> PMID: 18775316
5. Glotzer JB, Saffrich R, Glotzer M, Ephrussi A. 1997. Cytoplasmic flows localize injected *oskar* RNA in *Drosophila* oocytes. *Curr Biol* 7: 326–337. [https://doi.org/10.1016/s0960-9822\(06\)00156-4](https://doi.org/10.1016/s0960-9822(06)00156-4) PMID: 9115398
6. Ephrussi A, Lehmann R. 1992. Induction of germ cell formation by *oskar*. *Nature* 358: 387–392. <https://doi.org/10.1038/358387a0> PMID: 1641021
7. Smith JL, Wilson JE, Macdonald PM. 1992. Overexpression of *oskar* directs ectopic activation of *nanos* and presumptive pole cell formation in *Drosophila* embryos. *Cell* 70: 849–859. [https://doi.org/10.1016/0092-8674\(92\)90318-7](https://doi.org/10.1016/0092-8674(92)90318-7) PMID: 1516136
8. Chang CW, Nashchekin D, Wheatley L, Irion U, Dahlgard K, Montague TG, et al. 2011. Anterior-posterior axis specification in *Drosophila* oocytes: identification of novel *bicoid* and *oskar* mRNA localization factors. *Genetics* 188: 883–896. <https://doi.org/10.1534/genetics.111.129312> PMID: 21625003
9. Ephrussi A, Dickinson LK, Lehmann R. 1991. *Oskar* organizes the germ plasm and directs localization of the posterior determinant *nanos*. *Cell* 66: 37–50. [https://doi.org/10.1016/0092-8674\(91\)90137-n](https://doi.org/10.1016/0092-8674(91)90137-n) PMID: 2070417
10. Shapiro RS, Anderson KV. 2006. *Drosophila* *lk2*, a member of the I kappa B kinase family, is required for mRNA localization during oogenesis. *Development* 133: 1467–1475. <https://doi.org/10.1242/dev.02318> PMID: 16540511
11. Lehmann R, Nüsslein-Volhard C. 1986. Abdominal segmentation, pole cell formation, and embryonic polarity require the localized activity of *oskar*, a maternal gene in *Drosophila*. *Cell* 47: 141–152. [https://doi.org/10.1016/0092-8674\(86\)90375-2](https://doi.org/10.1016/0092-8674(86)90375-2) PMID: 3093084
12. Nüsslein-Volhard C, Frohnhofer HG, Lehmann R. 1987. Determination of anteroposterior polarity in *Drosophila*. *Science* 238: 1675–1681. <https://doi.org/10.1126/science.3686007> PMID: 3686007
13. Manseau L, Calley J, Phan H. 1996. Profilin is required for posterior patterning of the *Drosophila* oocyte. *Development* 122: 2109–2116. PMID: 8681792
14. Micklem DR, Adams J, Grünert S, St Johnston D. 2000. Distinct roles of two conserved Stauf domains in *oskar* mRNA localization and translation. *EMBO J* 19: 1366–1377. <https://doi.org/10.1093/emboj/19.6.1366> PMID: 10716936
15. Breitwieser W, Markussen FH, Horstmann H, Ephrussi A. 1996. *Oskar* protein interaction with *Vasa* represents an essential step in polar granule assembly. *Genes Dev* 10: 2179–2188. <https://doi.org/10.1101/gad.10.17.2179> PMID: 8804312
16. Lasko PF, Ashburner M. 1990. Posterior localization of *Vasa* protein correlates with, but is not sufficient for, pole cell development. *Genes Dev* 4: 905–921. <https://doi.org/10.1101/gad.4.6.905> PMID: 2384213
17. Wang C, Lehmann R. 1991. *Nanos* is the localized posterior determinant in *Drosophila*. *Cell* 66: 637–647. [https://doi.org/10.1016/0092-8674\(91\)90110-k](https://doi.org/10.1016/0092-8674(91)90110-k) PMID: 1908748
18. Kim-Ha J, Kerr K, Macdonald PM. 1995. Translational regulation of *oskar* mRNA by Bruno, an ovarian RNA-binding protein, is essential. *Cell* 81: 403–412. [https://doi.org/10.1016/0092-8674\(95\)90393-3](https://doi.org/10.1016/0092-8674(95)90393-3) PMID: 7736592
19. Lehmann R. 2016. Germ plasm biogenesis—an *Oskar*-centric perspective. *Curr Top Dev Biol* 116: 679–707. <https://doi.org/10.1016/bs.ctdb.2015.11.024> PMID: 26970648
20. Webster PJ, Liang L, Berg CA, Lasko P, Macdonald PM. 1997. Translational repressor Bruno plays multiple roles in development and is widely conserved. *Genes Dev* 11: 2510–2521. <https://doi.org/10.1101/gad.11.19.2510> PMID: 9334316
21. Nakamura A, Sato K, Hanyu-Nakamura K. 2004. *Drosophila* Cup is an eIF4E binding protein that associates with Bruno and regulates *oskar* mRNA translation in oogenesis. *Dev Cell* 6: 69–78. [https://doi.org/10.1016/s1534-5807\(03\)00400-3](https://doi.org/10.1016/s1534-5807(03)00400-3) PMID: 14723848
22. Chekulaeva M, Hentze MW, Ephrussi A. 2006. Bruno acts as a dual repressor of *oskar* translation, promoting mRNA oligomerization and formation of silencing particles. *Cell* 124: 521–533. <https://doi.org/10.1016/j.cell.2006.01.031> PMID: 16469699

23. Besse F, López de Quinto S, Marchand V, Trucco A, Ephrussi A. 2009. *Drosophila* PTB promotes formation of high-order RNP particles and represses *oskar* translation. *Genes Dev* 23: 195–207. <https://doi.org/10.1101/gad.505709> PMID: 19131435
24. Kim G, Pai C-I, Sato K, Person MD, Nakamura A, Macdonald PM. 2015. Region-specific activation of *oskar* mRNA translation by inhibition of Bruno-mediated repression. *PLoS Genet* 11(2): e1004992. <https://doi.org/10.1371/journal.pgen.1004992> PMID: 25723530
25. Reveal B, Yan N, Snee MJ, Pai CI, Gim Y, Macdonald PM. 2010. BREs mediate both repression and activation of *oskar* mRNA translation and act in trans. *Dev Cell* 18: 496–502. <https://doi.org/10.1016/j.devcel.2009.12.021> PMID: 20230756
26. Macdonald PM, Kanke M, Kenny A. 2016. Community effects in regulation of translation. *eLife* 5: e10965. <https://doi.org/10.7554/eLife.10965> PMID: 27104756
27. Kim-Ha J, Smith JL, Macdonald PM. 1991. *oskar* mRNA is localized to the posterior pole of the *Drosophila* oocyte. *Cell* 66: 23–35. [https://doi.org/10.1016/0092-8674\(91\)90136-m](https://doi.org/10.1016/0092-8674(91)90136-m) PMID: 2070416
28. Munro TP, Kwon S, Schnapp BJ, St Johnston D. 2006. A repeated IMP-binding motif controls *oskar* mRNA translation and anchoring independently of *Drosophila melanogaster* IMP. *J Cell Biol* 172: 577–588. <https://doi.org/10.1083/jcb.200510044> PMID: 16476777
29. Wilson JE, Connell JE, Macdonald PM. 1996. *aubergine* enhances *oskar* translation in the *Drosophila* ovary. *Development* 122: 1631–1639. PMID: 8625849
30. Chang JS, Tan L, Schedl P. 1999. The *Drosophila* CPEB homolog, *orb*, is required for Oskar protein expression in oocytes. *Dev Biol* 215: 91–106. <https://doi.org/10.1006/dbio.1999.9444> PMID: 10525352
31. Tomancak P, Berman BP, Beaton A, Weiszmann R, Kwan E, Hartenstein V, et al. 2007. Global analysis of patterns of gene expression during *Drosophila* embryogenesis. *Genome Biol*. 8: R145. <https://doi.org/10.1186/gb-2007-8-7-r145> PMID: 17645804
32. Liu N, Lasko P. 2015. Analysis of RNA interference lines identifies new functions of maternally-expressed genes involved in embryonic patterning in *Drosophila melanogaster*. *G3 (Bethesda)* 5: 1025–1034.
33. Bohne A, Darras A, D’Cotta H, Baroiller JF, Galiana-Arnoux D, Voff JN. 2010. The vertebrate makorin ubiquitin ligase gene family has been shaped by large-scale duplication and retroposition from an ancestral gonad-specific, maternal-effect gene. *BMC Genomics* 11: 721. <https://doi.org/10.1186/1471-2164-11-721> PMID: 21172006
34. Kim JH, Park SM, Kang MR, Oh SY, Lee TH, Muller MT, et al. 2005. Ubiquitin ligase MKRN1 modulates telomere length homeostasis through a proteolysis of hTERT. *Genes Dev* 19: 776–781. <https://doi.org/10.1101/gad.1289405> PMID: 15805468
35. Lee EW, Lee MS, Camus S, Ghim J, Yang MR, Oh W, et al. 2009. Differential regulation of p53 and p21 by MKRN1 E3 ligase controls cell cycle arrest and apoptosis. *EMBO J* 28: 2100–2113. <https://doi.org/10.1038/emboj.2009.164> PMID: 19536131
36. Lee MS, Han HJ, Han SY, Kim IY, Chae S, Lee CS, et al. 2018. Loss of the E3 ubiquitin ligase MKRN1 represses diet-induced metabolic syndrome through AMPK activation. *Nat Commun* 9: 3404 <https://doi.org/10.1038/s41467-018-05721-4> PMID: 30143610
37. Cassar PA, Carpenedo RL, Samavarchi-Tehrani P, Olsen JB, Park CJ, Chang WY, et al. 2015. Integrative genomics positions MKRN1 as a novel ribonucleoprotein within the embryonic stem cell gene regulatory network. *EMBO Rep* 10: 1334–1357.
38. Carpenedo RL, Cassar PA, Stanford WL. 2016. MKRN1: Uncovering function by an unbiased systems approach. *Cell Cycle* 15: 303–304. <https://doi.org/10.1080/15384101.2015.1124698> PMID: 26651844
39. Miroci H, Schob C, Kindler S, Olschlager-Schutt J, Fehr S, Jungenitz T, et al. 2012. Makorin ring zinc finger protein 1 (MKRN1), a novel poly(A)-binding protein-interacting protein, stimulates translation in nerve cells. *J Biol Chem* 287: 1322–1334. <https://doi.org/10.1074/jbc.M111.315291> PMID: 22128154
40. Vazquez-Pianzola P, Urlaub H, Suter B. 2011. pAbp binds to the *osk* 3’UTR and specifically contributes to *osk* mRNA stability and oocyte accumulation. *Dev Biol* 357: 404–418. <https://doi.org/10.1016/j.ydbio.2011.07.009> PMID: 21782810
41. Winslow GM, Carroll SB, Scott MP. 1988. Maternal-effect genes that alter the fate map of the *Drosophila* blastoderm embryo. *Dev Biol* 129: 72–83. [https://doi.org/10.1016/0012-1606\(88\)90162-5](https://doi.org/10.1016/0012-1606(88)90162-5) PMID: 3410162
42. Rongo C, Gavis ER, Lehmann R. 1995. Localization of *oskar* RNA regulates *oskar* translation and requires Oskar protein. *Development* 121: 2737–2746. PMID: 7555702
43. Nakamura A, Amikura R, Hanyu K, Kobayashi S. 2001. Me31B silences translation of oocyte-localizing RNAs through the formation of cytoplasmic RNP complex during *Drosophila* oogenesis. *Development* 128: 3233–3242. PMID: 11546740

44. Norvell A, Debec A, Finch D, Gibson L, Thoma B. 2005. Squid is required for efficient posterior localization of *oskar* mRNA during *Drosophila* oogenesis. *Dev Genes Evol* 215: 340–349. <https://doi.org/10.1007/s00427-005-0480-2> PMID: 15791421
45. Steinhauer J, Kalderon D. 2005. The RNA-binding protein Squid is required for the establishment of anteroposterior polarity in the *Drosophila* oocyte. *Development* 132: 5515–5525. <https://doi.org/10.1242/dev.02159> PMID: 16291786
46. Geng C, Macdonald PM. 2006. Imp associates with Squid and Hrp48 and contributes to localized expression of Gurken in the oocyte. *Mol Cell Biol* 26: 9508–9516. <https://doi.org/10.1128/MCB.01136-06> PMID: 17030623
47. Clouse KN, Ferguson SB, Schüpbach T. 2008. Squid, Cup, and PABP55B function together to regulate *gurken* translation in *Drosophila*. *Dev Biol* 313: 713–724. <https://doi.org/10.1016/j.ydbio.2007.11.008> PMID: 18082158
48. McDermott SM, Meignin C, Rappsilber J, Davis I. 2012. *Drosophila* Syncrin binds the *gurken* mRNA localisation signal and regulates localised transcripts during axis specification. *Biol Open* 1: 488–497. <https://doi.org/10.1242/bio.2012885> PMID: 23213441
49. Hildebrandt A, Brüggemann M, Rücklé C, Boerner S, Heidelberger JB, Busch A, et al. 2019. The RNA-binding ubiquitin ligase MKRN1 functions in ribosome-associated quality control of poly(A) translation. *Genome Biol* 20: 216 <https://doi.org/10.1186/s13059-019-1814-0> PMID: 31640799
50. Lee FCY and Ule J. 2018. Advances in CLIP Technologies for Studies of Protein-RNA Interactions. *Mol Cell* 69:354–369 <https://doi.org/10.1016/j.molcel.2018.01.005> PMID: 29395060
51. Jenny A, Hachet O, Závorszky P, Cyrklaff A, Weston MDJ, St Johnston D, et al. 2006. A translation-independent role of *oskar* RNA in early *Drosophila* oogenesis. *Development* 133: 2827–2833. <https://doi.org/10.1242/dev.02456> PMID: 16835436
52. Schüpbach T, Wieschaus E. 1991. Female sterile mutations on the second chromosome of *Drosophila melanogaster*. *Genetics* 129: 1119–1136. PMID: 1783295
53. Jeong EB, Jeong SS, Cho E, Kim EY. 2019. Makorin 1 is required for *Drosophila* oogenesis by regulating insulin/Tor signaling. *PLoS ONE* 14(4): e0215688. <https://doi.org/10.1371/journal.pone.0215688> PMID: 31009498
54. Castagnetti S, Ephrussi A. 2003. Orb and a long poly(A) tail are required for efficient *oskar* translation at the posterior pole of the *Drosophila* oocyte. *Development* 130: 835–843. <https://doi.org/10.1242/dev.00309> PMID: 12538512
55. Ryu YH, Macdonald PM. 2015. RNA sequences required for the noncoding function of *oskar* RNA also mediate regulation of Oskar protein expression by Bicoid Stability Factor. *Dev Biol* 407: 211–223. <https://doi.org/10.1016/j.ydbio.2015.09.014> PMID: 26433064
56. Filardo P, Ephrussi A. 2003. Bruno regulates *gurken* during *Drosophila* oogenesis. *Mech Dev* 120: 289–297. [https://doi.org/10.1016/s0925-4773\(02\)00454-9](https://doi.org/10.1016/s0925-4773(02)00454-9) PMID: 12591598
57. Reveal B, Garcia C, Ellington A, Macdonald PM. 2011. Multiple RNA binding domains of Bruno confer recognition of diverse binding sites for translational repression. *RNA Biol* 8: 1047–1060. <https://doi.org/10.4161/rna.8.6.17542> PMID: 21955496
58. Qian X, Wang L, Zheng B, Shi ZM, Ge X, Jiang CF, et al. 2016. Deficiency of Mkrn2 causes abnormal spermiogenesis and spermiation, and impairs male fertility. *Sci Rep* 6: 39318. <https://doi.org/10.1038/srep39318> PMID: 28008940
59. Lécuyer E, Parthasarathy N, Krause HM. 2008. Fluorescent in situ hybridization protocols in *Drosophila* embryos and tissues. *Methods Mol Biol* 420: 289–302. https://doi.org/10.1007/978-1-59745-583-1_18 PMID: 18641955
60. Lence T, Akhtar J, Bayer M, Schmid K, Spindler L, Ho CH, et al. 2016. m⁶A modulates neuronal functions and sex determination in *Drosophila*. *Nature* 540: 242–247. <https://doi.org/10.1038/nature20568> PMID: 27919077
61. Na H, Laver JD, Jeon J, Singh F, Ancevicus K, Fan Y, et al. 2016. A high-throughput pipeline for the production of synthetic antibodies for analysis of ribonucleoprotein complexes. *RNA* 22: 636–655. <https://doi.org/10.1261/rna.055186.115> PMID: 26847261
62. Hildebrandt A, Alanis-Lobato G, Voigt A, Zarnack K, Andrade-Navarro MA, Beli P, et al. 2017. Interaction profiling of RNA-binding ubiquitin ligases reveals a link between posttranscriptional regulation and the ubiquitin system. *Sci Rep* 7: 16582. <https://doi.org/10.1038/s41598-017-16695-6> PMID: 29185492
63. Ritchie ME, Phipson B, Wu D, Hu Y, Law CW, Shi W, et al. 2015. limma powers differential expression analyses for RNA-sequencing and microarray studies. *Nucleic Acids Res* 43: e47. <https://doi.org/10.1093/nar/gkv007> PMID: 25605792
64. Wickham H. 2016. ggplot2: Elegant Graphics for Data Analysis. Springer-Verlag New York.

65. Ebersberger I, Simm S, Leisegang MS, Schmitzberger P, Mirus O, von Haeseler A, et al. 2014. The evolution of the ribosome biogenesis pathway from a yeast perspective. *Nucleic Acids Res* 42: 1509–1523. <https://doi.org/10.1093/nar/gkt1137> PMID: 24234440
66. Sonnhammer EL, Gabaldón T, Sousa da Silva AW, Martin M, Robinson-Rechavi M, Boeckmann B, et al. 2014. Big data and other challenges in the quest for orthologs. *Bioinformatics* 30: 2993–2998. <https://doi.org/10.1093/bioinformatics/btu492> PMID: 25064571
67. Koestler T, von Haeseler A, Ebersberger I. 2010. FACT: functional annotation transfer between proteins with similar feature architectures. *BMC Bioinformatics* 11: 417. <https://doi.org/10.1186/1471-2105-11-417> PMID: 20696036
68. Katoh K, Standley DM. 2013. MAFFT multiple sequence alignment software version 7: improvements in performance and usability. *Mol Biol Evol* 30: 772–780. <https://doi.org/10.1093/molbev/mst010> PMID: 23329690
69. Sutandy FX, Hildebrandt A, König J. 2016. Profiling the binding sites of RNA-binding proteins with nucleotide resolution using iCLIP. *Methods Mol Biol* 1358: 175–195. https://doi.org/10.1007/978-1-4939-3067-8_11 PMID: 26463384
70. Dodt M, Roehr JT, Ahmed R, and Dieterich C. 2012. Flexbar—flexible barcode and adapter processing for next-generation sequencing platforms. *MDPI Biology*, 1(3): 895–905.
71. Aken BL, Achuthan P, Akanni W, Amode MR, Bernsdorff F, Bhai J, et al. 2017. Ensembl 2017. *Nucleic Acids Res* 45: D635–D642. <https://doi.org/10.1093/nar/gkw1104> PMID: 27899575
72. Dobin A, Davis CA, Schlesinger F, Drenkow J, Zaleski C, Jha S, et al. 2013. STAR: ultrafast universal RNA-seq aligner. *Bioinformatics* 29: 15–21. <https://doi.org/10.1093/bioinformatics/bts635> PMID: 23104886
73. Li H, Handsaker B, Wysoker A, Fennell T, Ruan J, Homer N, et al. 2009. The Sequence Alignment/Map format and SAMtools. *Bioinformatics* 25: 2078–2079. <https://doi.org/10.1093/bioinformatics/btp352> PMID: 19505943
74. Quinlan AR, Hall IM. 2010. BEDTools: a flexible suite of utilities for comparing genomic features. *Bioinformatics* 26: 841–842. <https://doi.org/10.1093/bioinformatics/btq033> PMID: 20110278
75. Kent WJ, Zweig AS, Barber G, Hinrichs AS, Karolchik D. 2010. BigWig and BigBed: enabling browsing of large distributed data sets. *Bioinformatics* 26: 2204–2207. <https://doi.org/10.1093/bioinformatics/btq351> PMID: 20639541
76. Edgar R, Domrachev M, Lash AE. 2002. Gene Expression Omnibus: NCBI gene expression and hybridization array data repository. *Nucleic Acids Res* 30: 207–210. <https://doi.org/10.1093/nar/30.1.207> PMID: 11752295